REVIEW OF NUCLEAR WEAPONS EFFECTS[1]

By Harold L. Brode[2]
The RAND Corporation, Santa Monica, California

CONTENTS

Introduction

The purpose of this paper is to review nuclear explosion physics and to provide formulas for estimating the various transient phenomena. Since in many cases the available formulas are quite empirical, a sketchy physical background is included. Nuclear explosions provide access to a realm of high-temperature, high-pressure physics not otherwise available on a macroscopic scale on earth. The application of nuclear explosions to destruction and warfare is well known, but as in many other fields of research, out of the study of nuclear explosions other new and seemingly unrelated developments have come. In fact, physicists find plenty of interesting and novel physics in the environment of a nuclear explosion. Some of the physical phenomena are valuable objects of research, and promise to provide further understanding of nature.

[1] The survey of literature for this review was concluded in March 1968.

[2] Any views expressed in this paper are those of the author. They should not be interpreted as reflecting the views of The RAND Corporation or the official opinion or policy of any of its government or private research sponsors.

Of more immediate practicality, many of the explosion features have important consequences for the design and provision of shelter for wartime use. Most military systems and systems analysts have been heavily influenced by the use of or protection from nuclear explosions. Modern nations consider nuclear explosion phenomena in providing wartime protection for their people. The United States, for largely political reasons, has done less toward providing shelter for civilians than many other countries, yet it has sponsored a great deal of research into the effects of nuclear weapons, and can provide detailed guidance on appropriate protective measures.

The official unclassified nuclear weapons effects source is an excellent and lengthy compendium *The Effects of Nuclear Weapons* [edited by Glasstone (1)], but even that is unable to treat all effects in equal detail. The present paper differs in at least two important ways: (*a*) it emphasizes simple approximations and prediction techniques, and (*b*) it concentrates on close-in phenomena pertinent to high levels of protection and vital to the understanding of crater formation, ground shock, fireball effects, cloud behavior, thermal radiation, and debris and fallout. It is also a great deal briefer.

In the process of this review, a few of the more startling and nonintuitive features of nuclear effects will be disclosed, and hopefully may become more understandable: the bright light of a nuclear detonation is extinguished temporarily before much of the energy has shone out; at certain distances, trees or buildings will fall toward the point of explosion rather than away from it; and the electromagnetic signal generated by a nuclear burst has contributions at frequencies from fractions of a cycle per second to kilomega-Hertz.

The review deals separately with such features as the fireball, the nuclear radiation, the thermal radiation, the electromagnetic pulse (EMP), cratering, ground shock, the air blast, ejecta, and fallout. While this is a logical subdivision of nuclear burst phenomenology, all of these factors are thoroughly interdependent. The quick sequence of events in a nuclear explosion begins with the nuclear reactions and their radiations inside the weapon, but both the prompt radiation doses some distance away and the subsequent fallout activity carried to much larger distances are influenced greatly by the dynamics of the explosion. The shocked air and the violent expansion of the heated fireball dictate the nature of the thermal radiation both early and late. At the same time, the cratering action puts vast amounts of earth material into the early fireball, thus further influencing the thermal radiation and the fallout. All effects begin with the nuclear reactions and their radiations, and all those listed are affected by the blast. Many features, in turn, have some influence on the blast itself.

Although the design of a nuclear weapon might lead to differences in the explosion phenomena, none of the major weapon effects is critically dependent on such weapon detail. The neutron and gamma-ray doses, the fallout, and the EMP all have rather direct connections with the weapon neutronics, but useful estimates can be made without recourse to specific information

about weapons construction or operation. A source for the fireball, blast, and thermal radiation phenomena for atmospheric bursts need contain no weapon model. In less than the first microsecond most of the explosion energy has escaped into an air mass many times the mass of the weapon, and from then on the blast and thermal features can be expressed independently of any bomb model.

The Source of It All

The yields and the energy densities for modern weapons range over many orders of magnitude. The yields may range from fractions of a kiloton to tens or even hundreds of thousands of kilotons, i.e., into the 100-MT (megaton) range. These enormous ranges of energies are not matched by comparable ranges in the mass required in the weapons, so that the yield-to-mass ratio may likely change by quite large fractions. Thus we can expect that the energy density or the mean temperature of the bomb vapors at the time of the release of nuclear energy may have a comparable wide range. Typically, the exterior of a weapon may reach peak temperatures of tens of millions of degrees Centigrade.

The initial radiations from a nuclear weapon (i.e., the gamma rays and neutrons, and the X-ray radiations from the extremely high temperatures of the bomb vapors) are largely determined by the bomb materials and the construction of the nuclear weapon itself and not by the external environment. Thus, whether the explosion takes place in the atmosphere, out in space, underwater, or underground does not matter much in the achievement of the initial energy densities and radiative properties. This is not strictly true in every environment, but provided the immediate surroundings are not as dense as the weapon itself, the fraction of energy which may be radiated out as X rays before the bomb begins to blow apart under hydrodynamic action depends largely on its yield-to-mass ratio and to some extent on its construction detail. This fraction may range from almost nothing at all (or a very small per cent) to significantly more than 80 per cent of the total energy generated.

One can estimate the energy density or an average temperature for a bomb of yield W KT (kilotons) (10^{12} cal/KT), mass M, and radius R, assuming only that the energy is generated instantaneously and that the bomb vapors rapidly reach thermodynamic equilibrium and equilibrium with the radiation field. The energy released in the nuclear reactions is largely in fast recoiling nuclear matter. Most of these nuclei, being charged particles, have very short ranges and thermalize with the surrounding atomic matter very quickly. Only the uncharged products (neutrons, gamma rays, neutrinos) can expect to escape from the explosive mass, and even there most of the fission gamma rays will be absorbed and a large fraction of the neutrons may be thermalized and captured. The temperatures to be expected are in the tens of millions of degrees Kelvin, i.e., in the kilovolt (keV) range, so that the radiation energy density can be comparable to the material energy

density. Thus, the energy density should be written with two terms, such as

$$E = C_v T + aT^4/\rho \qquad \text{(ergs/g)} \qquad 1.$$

in which a is the radiation constant (0.7563^{-14} ergs/cm^3/(°K)^4, [3] ρ is the average density (g/cm^3), and C_v is the effective specific heat of the bomb vapors. Since these vapors at high temperatures are likely to form a plasma of electrons and completely stripped atoms, the ideal gas specific heat (3/2) nR/(mol wt) is a fair approximation, with $n \simeq Z+1$, and Z being an average atomic number for the bomb materials. Since the ratio $(Z+1)$/(mol wt) is approximately one half for any material, the specific heat (C_v) is approximately $3R/4 \simeq 6.24^{+7}$ ergs/g °K. The energy density can be approximated, then, as

$$E \simeq 6.2^{+7}T + 7.6^{-18}(T)^4/\rho \qquad \text{(ergs/g)} \qquad 2.$$

with T in °K and ρ in g/cm^3.

The average energy density can be expressed also as the total yield divided by the total mass, and the density is the mass divided by the volume, so that Equation 2 can be rewritten as

$$W = 0.78M\phi + 0.39R^3\phi^4 \qquad 3.$$

in which M is the bomb mass (in hundreds of pounds), ϕ is the "average" temperature (in keV), R is the radius (in feet), and W is the yield (in KT).

An example or two will show the appropriate range of average temperatures. For instance, 1 KT in 100 pounds at a density of 2.7 g/cm^3 ($R = 0.5213$ ft) gives an average temperature of 1.18 keV. This agrees with the value obtained for an aluminum sphere with the same mass and yield [Brode et al. (2)]. In this example, very little of the energy (11 per cent) is in the radiation field. Even so, because the radiation energy is highly mobile, an appreciably larger fraction of the total energy can be transported out of the bomb mass by radiation diffusion.

With 50 times more energy, the temperature would rise to about 5 keV, and nearly all the energy (93 per cent) could be in the radiation. However, the fourth-power dependence on temperature for the radiation energy density allows only slight temperature increases to match big increases in energy density. Thus, if the yield were 200 times larger (200 KT), the temperature would rise to only about 7 keV.

At the higher temperatures, most of the bomb vapor atoms become completely ionized (stripped), and photons are subject only to Compton scattering (little absorption). The bomb vapors thus become relatively transparent and once the whole mass is heated to high temperature, any subsequent energy introduced diffuses out into the surrounding air nearly as fast as it is generated. As the vapors cool, however, there comes a temperature and a time when their increasing opacity (as electrons reattach) slows down the

[3] The shorthand mathematical notation for powers of ten is used here, so that $0.7563^{-14} \equiv 0.7563 \times 10^{-14}$.

diffusion of radiation so much that hydrodynamics becomes the more important mechanism for transferring any remaining energy in the bomb to its surroundings.

In the aluminum sphere example, for which only 30 per cent of the 1-KT total energy was radiated into the air, 10 per cent was out in little over 0.1 μsec, 20 per cent in less than 0.2 μsec, and nearly 30 per cent by 0.4 μsec. Although, by 0.4 μsec, the vapors had expanded to a radius only 1.6 times larger than the initial radius, roughly one-third the energy was already in kinetic energy, with the other two thirds split about evenly between the heat left in the aluminum vapors and the internal energy dumped in the surrounding air by the radiation diffusion. Much later, at 1 μsec, about half the energy still remained in the aluminum vapors, but all of it was in kinetic energy, and very little more energy had been (or would be) transferred to the air by radiation. The kinetic energy is used up in doing work on the surrounding air, but that takes much longer.

The Fireball—Radiative Growth

The energy which does escape as X rays in this early phase does not escape far from atmospheric explosions, because X rays in this range of a few tens of millions of degrees Kelvin are rather "soft." X rays of 1 or 2 kV energy have mean free paths in air that are quite short (1/4 to 2 cm) (3); consequently, they are absorbed in the air immediately around the bomb. The cold air absorption mean free path for X rays in air can be approximated (above the K edges, i.e., above $\sim$0.55 keV) by $\lambda \simeq \eta/4\ (h\nu)^{2.78}$ cm where $\eta = \rho/\rho_0$, $\rho_0 = 1.293^{-3}$ g/cm^3, and $h\nu$, the photon energy, is in keV. However, as the air around the bomb is heated to very high temperatures it, too, becomes less absorbent. That is, the air atoms become hotter and their absorption properties become those of a completely ionized plasma in which the X rays are subjected to Compton scatterings only. In general, the hot air becomes transparent to X rays at a lower temperature than that at which the bomb vapors do. Thus, even when the bomb vapors have grown too cold to radiate efficiently, the heating of the air by the then rapidly expanding bomb material continues to feed the radiative growth of the early fireball. The shock caused by these expanding vapors is not adiabatic, but is more nearly isothermal, since as fast as the shock compresses and heats more of the fireball air, it radiates the added energy out through the hot fireball into the cold air beyond.

Table I indicates that relatively small spheres of air contain quite large amounts of energy at the high temperatures created by these X-ray emanations. These temperatures are too high for the air to remain that hot for very long. In fact, at the higher temperatures, there is more energy in the radiation field than in the electrons and ions of the air plasma. Although the radiation is not in exact equilibrium with the air during this earliest fireball growth, these radii represent the size and temperatures of the earliest (X-ray) fireball.

TABLE I

SIZE OF SPHERES OF SEA LEVEL AIR NECESSARY TO CONTAIN 1 KT, 1 MT, OR 100 MT OF ENERGY AT VARIOUS UNIFORM TEMPERATURES

Temperature millions of °C	Radius for hot air sphere		
	1 KT	1 MT	100 MT
7.5	.75 m	7.5 m	35 m
6	1	10	46
5	1.25	12	57
4	1.6	16	74
3	2.1	21	100

In the next few microseconds this air reradiates very rapidly into the cold air, and the fireball grows by radiation diffusion.

A typical temperature and density profile at an early time (34 μsec) is illustrated in Figure 1. The highest temperature within the hot sphere is less than twice that near the outer edge (at 40 m), but it then drops rapidly in a sharp front. In the same figure, the density curve shows the air relatively little changed from its ambient condition beyond 10 m. In fact, at this time there is only a slight compression at the front of the fireball and a slight rarefaction, or reduction in density, in the interior. But the figure shows a high compression or shock within the bomb materials which, at this time of 34 μsec, have expanded out to a thin shell at 10 m.

Figure 2 illustrates the distribution of pressure and of velocity at this same time (34 μsec) for this 1-MT sea level example. The pressure profile is similar to the temperature profile within the hot air, but shows much higher pressure in the bomb vapor shock wave. Similarly, the bomb material is

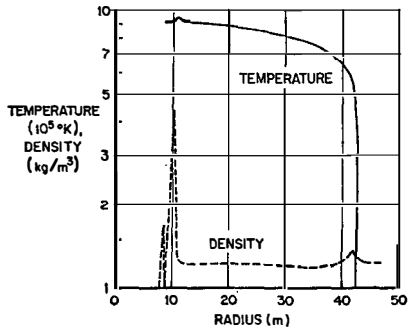

FIG. 1. Early fireball temperature and density profiles (1 MT-sea level-air burst, time≃34 μs).

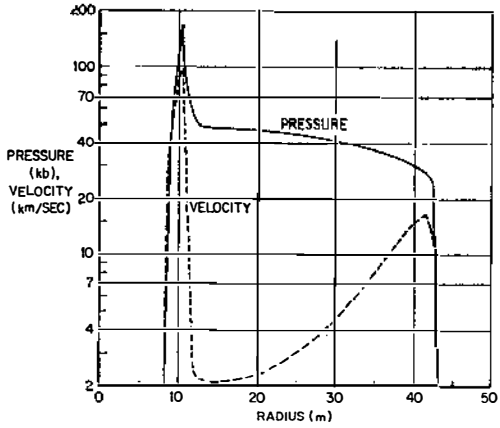

FIG. 2. Early fireball pressure and particle velocity profiles (1 MT-sea level-air burst, time ~34 μs).

een to be expanding at an extremely high velocity, while the air out in the est of the fireball is just beginning to move. This rapidly expanding sphere f bomb vapors picks up the adjacent air and compresses it manyfold in a onadiabatic, nearly isothermal shock. The expanding shell can squeeze up ıe air to many times the density achievable in a classical adiabatic shock ecause most of the energy (and pressure) the compressed air acquires in eing shocked is immediately radiated out ahead through the transparent reball interior.

Figure 3 illustrates, on a logarithmic plot, a typical dependence of the arious fronts on radius and time. The radiation front itself expands at the arliest fractions of a microsecond to tens of meters. Then its rate of expan- on drops suddenly as the energy from the nuclear reactions stops and the emaining heat in the bomb is no longer free to radiate out because of the

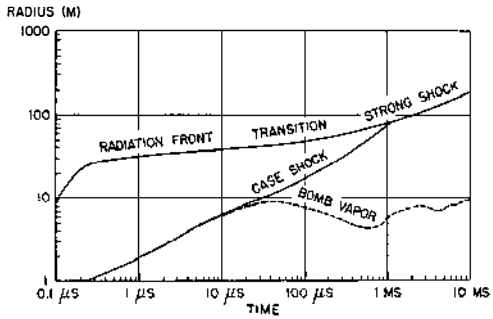

FIG. 3. Space-time plot of early phase fireball (1 MT-sea level-air burst).

increasing opacity of the vapors as their temperature drops. At the san times, one sees the bomb itself expanding in what is labeled the *case shoc* Ultimately, the bomb vapors drop behind as more and more air is picked u and this inner shock moves away. The case shock then chases out throug the hot fireball as the outer edge of the fireball begins also to form a shoc

Each of these features—the radiation expansion front, the transition a shock front at that fireball front, the expansion of the bomb vapors, ar the generation of the case shock—may be expected to scale differently f different weapons, for different yields, and for different altitudes of burs If the design of the weapon allowed less radiation out or more radiation remain in the case, then the point of intersection of these two shocks wou surely be changed, although the yield of the explosion and the altitude burst may be the same.

Fireball—Transition from Radiative to Shock Growth

Figure 4 shows subsequent temperature profiles as the radiation sphe of the early fireball ceases to expand solely by radiation diffusion and begi to "shock up," and to grow by compressing and doing work on the surroun ing air. In this semilogarithmic plot of temperature versus range for vario times (Figure 4), one sees at the earliest indicated time the temperature the radiation diffusion sphere. At subsequent times, this radiatively heat region is shown to be expanded and cooled as it follows the shock wave, ar one sees the shock-heated air as a region of steep temperature gradient b yond the hot interior. At these times, the lowest temperature within tl fireball is at the fireball surface, or in the outer shock front itself. The visib fireball radius becomes coincident with this shock front after the first mil second.

In Figure 5 the relative air densities are shown in a similar semilogarit

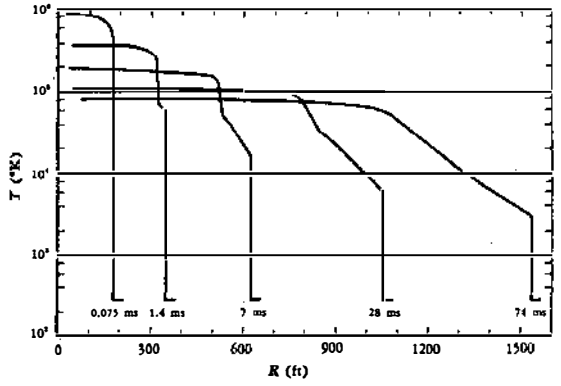

Fig. 4. Fireball temperature versus radius at early times in the fireball history (1 MT-surface burst).

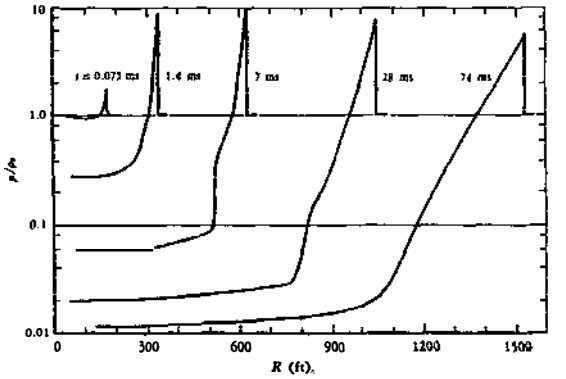

FIG. 5. Fireball density versus radius at early times in the fireball history (1 MT-surface burst).

mic plot for the same times. Here, at the earliest times, relatively little compression or expansion has taken place since radiation has been the mechanism for fireball growth. However, at subsequent times the developing shock expands and compresses more and more of the air. The hot interior region drops to lower and lower densities—ultimately to densities (for such a megaton sea level burst) of about 1 per cent of the normal atmospheric density.

Figure 6 illustrates this fireball growth transition from a radiation wave

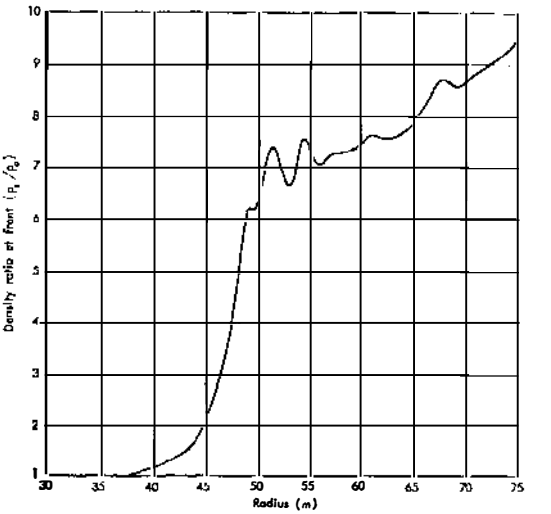

FIG. 6. Fireball transition from radiation diffusion growth to shock (1 MT).

to a shock wave. It shows as a function of radius the increase of density at the front, which ultimately becomes the shock front. As Figure 6 indicates, the growth of the shock wave out of this radiation wave does not occur at a single radius but is a gradual process developing over some fair fraction of the "initial" or radiative growth radius. Even after a shock wave is formed the temperatures at the front are still quite high, being close to one hundred thousand degrees Kelvin or ten electron volts.

Because the transition from radiative growth to a shock expansion illustrated in Figure 6 depends on both hydrodynamic features and radiative properties of the hot fireball, its scaling with altitude and yield could be quite complex. However, at sea level, as mentioned, transition occurs at nearly the same fireball temperature, so the volume of the fireball at the time of shock formation should scale only slightly slower than directly with the yield, i.e., the radius at shock formation should vary about as the cube root of the yield. The altitude or ambient density dependence is somewhat more complicated, and comes more from the change of absorption properties with density changes. An approximate scaling derived from a series of detailed calculations (4) goes as follows:

$$R_{\text{shock formation}} \simeq 47W^{.324}(\rho/\rho_0)^{-1/2} \text{ m} \pm 10 \text{ per cent} \qquad 4.$$

in which W is in MT, ρ is the density at altitude, and ρ_0 is the standard sea level air density. More accurate scaling of such features as this radius for transition should include the radiative or X-ray yield, since these can change both as functions of yield and of bomb design. The above approximation (± 10 per cent) covers most of the available calculations from 1 KT to 4 MT and from sea level to 100 kft.

Fireball—Shock Growth

Figure 7 illustrates the overpressures which occur for the same times as illustrated earlier in Figures 4 and 5 for the early temperature and density profiles from a megaton explosion. Here, again, one sees the bomb vapor

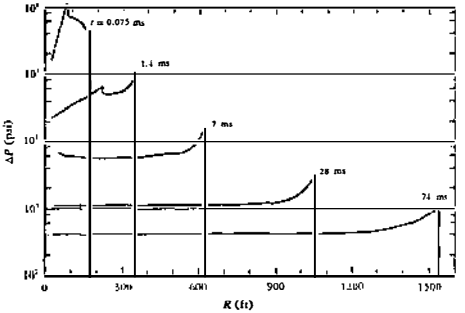

Fig. 7. Overpressure versus range at early times in the shock-wave growth (1 MT-surface burst).

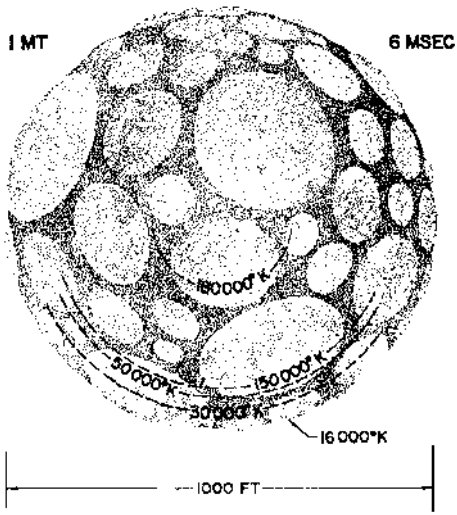

FIG. 8. Early fireball size and temperature (while shock front is opaque).

hock following the radiation front, the radiation front shocking up, the omb shock catching up and forming after a few milliseconds a pressure rofile typical of a classical strong shock wave. This simple form of the last ressure profiles of Figure 7 will persist to quite late times, even after the hock wave has become separated from the fireball.

Figure 8 is intended to illustrate the general features of photographs of a uclear explosion during this period when the shock wave forms the surface f the fireball. Often, the most striking feature of such photographs is the ack of complete symmetry or sphericity. There are frequent large blisters nd bright spots on the glassy-looking shock front. Quite likely, these are lobs of bomb vapors which are thrown at high velocities against the back of he shock wave. They are accelerated in the earliest phases of the weapon's xpansion and remain in dense clumps or jets while the fireball expands, and o are not subject to as much decelerating drag. Since the fireball expansion lows rapidly after its initial radiative growth, such blobs ultimately overtake he fireball front, splashing against the high density of the back of the shock. The steep gradients in temperature within the fireball are also illustrated in his figure, showing that although the shock front is the lowest temperature ne sees, the interior can still be at extremely high temperatures and yet ontinue to be obscured by the outer shock-heated air.

HYDRODYNAMIC SCALING

For most blast features from both nuclear and chemical explosions there xists a particularly simple transformation which allows their description to e scaled to fit that for other amounts of explosive or other energy releases.

With some restriction on the initial explosive density, a similarly simple scaling is appropriate for describing the effect on the blast of changing the ambient atmosphere into which it expands. The equations of motion appropriate to the shocks and hydrodynamic flow of a spherical blast are themselves scalable, i.e., can be put in dimensionless form with the reduced variables being related to the radial and temporal variables by simple scale factors. Provided that the boundary or initial conditions scale in the same way, the scaling can be quite rigorous. That the yield or energy scaling is valid over extreme ranges (from charges of a few grams of explosive to chemical charges in the hundreds of tons and nuclear explosions in the many millions of tons) confirms the appropriateness of such scaling. For many of the blast features, the nonscalable early radiation effects are unimportant.

To illustrate this scaling, consider the following set of equations which, together with a set of boundary conditions are sufficient to describe the blast wave. In these equations the mass per steradian is represented by M, the density by ρ, the radius by R, and time by t, the particle velocity by u, the pressure by P, the specific internal energy by E. Thus, $4\pi M = \frac{4}{3}\pi R^3 \rho$ and

$$\frac{1}{\rho} = R^2 \frac{\partial R}{\partial M} \quad \text{(conservation of mass)} \tag{5.}$$

$$\frac{\partial u}{\partial t} = -R^2 \frac{\partial P}{\partial M} \quad \text{(conservation of momentum)} \tag{6.}$$

$$\frac{\partial E}{\partial t} = \frac{P}{\rho^2} \frac{\partial \rho}{\partial t} \quad \text{(conservation of energy)} \tag{7.}$$

$$P(E, \rho) \text{ equation of state} \tag{8.}$$

In this Langrangian or mass coordinate formulation, the particle velocity is defined as

$$u = \frac{\partial R}{\partial t} \tag{9.}$$

If the explosion energy is Y_1 and the ambient atmosphere is characterized by pressure P_{01}, density ρ_{01}, energy E_{01}, and sound speed C_{01}, and if we choose a dimensionless length, time, and mass, such that

$$\begin{aligned} R &= \alpha\lambda \\ t &= \alpha\tau/C_{01} \\ M &= \rho_{01}\alpha^3 m \end{aligned} \tag{10.}$$

with

$$x^1 = Y_1/P_{01}$$

then the following dimensionless equations can be written from Equations 5–8 above.

$$\frac{1}{\eta} = \lambda^2 \frac{\partial \lambda}{\partial m} \tag{11.}$$

$$\frac{\partial \beta}{\partial \tau} = \frac{-\lambda^2}{\gamma_{01}} \frac{\partial \pi}{\partial m} \tag{12.}$$

$$\frac{\partial \epsilon}{\partial \tau} = (\gamma_{01} - 1) \frac{\pi}{\eta^3} \frac{\partial \eta}{\partial \tau} \tag{13.}$$

$$\frac{\partial \lambda}{\partial \tau} \equiv \beta \tag{14.}$$

n these equations the dependent variables are defined in units of their ımbient or preshock values, viz.;

$$\begin{aligned} \pi &= P/P_{01} \\ \eta &= \rho/\rho_{01} \\ \beta &= u/C_{01} \\ \epsilon &= E/E_{01} \\ \gamma_{01} &= P_{01}/(E_{01}\rho_{01}) + 1 \end{aligned} \tag{15.}$$

ınd are thus dimensionless. Solutions to these equations are then indepen-lent of the particular explosion energy and the appropriate ambient condi-ions.

For two explosions of energies Y_1 and Y_2 all these dimensionless hydro-lynamic variables are then the same at times and distances t_1 and R_1 for ·ield Y_1 and t_2 and R_2 for yield Y_2 when the ratio of radii and times is equal o the cube root of the ratio of the yields, i.e.,

$$R_1 = R_2(Y_1/Y_2)^{1/3} \tag{16.}$$

$$t_1 = t_2(Y_1/Y_2)^{1/3} \tag{17.}$$

For example, if, for a pressure ratio of two atmospheres ($P_2/P_{02} = 2$) from a :iloton nuclear burst (Y_2) the shock radius is 238 m (R_2) and the arrival ime is 0.3 sec (t_2), then for a megaton explosion the same pressure occurs ıt 2380 m and at 3 sec.

The altitude or ambient atmosphere scaling is nearly as simple, but is ıot as universally valid. If P_1 and P_2 are pressures at R_1, t_1, and R_2, t_2 and P_{01} and P_{02} are the ambient air pressure, the scaling is defined such that the ›ressure ratio (shock pressure relative to ambient) is the same, i.e.,

$$P_1/P_{01} = P_2/P_{02} \tag{18.}$$

vhen the shock radii are related as

$$R_1 = R_2(P_{02}/P_{01})^{1/3} \tag{19.}$$

When this is so, the times are related so that

$$t_1 = t_2(P_{02}/P_{01})^{1/3}(T_{02}/T_{01})^{1/2} \tag{20.}$$

If the ambient temperatures T_{01} and T_{02} (on an absolute scale) are differ-:nt, then the particle velocities, sound speeds, and times will be different by actors like the square root of the ratio of ambient temperatures. Thus, at he same scaled distances and times as above, the sound velocity (C), the ıbsolute temperature (T), the particle velocity (u), the shock velocity (U)

will be related for the explosions in the two atmospheres (P_{01} and P_{02}) by:

$$C_{01}/C_{02} = (T_{01}/T_{02})^{1/2} \quad (T \text{ in } °\text{K}) \tag{21.}$$

$$u_1/u_2 = C_{01}/C_{02} \tag{22.}$$

$$U_1/U_2 = C_{01}/C_{02} \tag{23.}$$

$$T_1/T_2 = T_{01}/T_{02} \tag{24.}$$

These ambient condition scaling relations [sometimes referred to as Sachs scaling (5)] are rigorously valid only for hydrodynamic motions, and only in cases when initial conditions either scale in the same way or can be ignored after some early time or outside of some small initial volume. For chemical explosives, the mass of charge is so great, or rather the energy density in the explosive products is so low, that at all except the lowest blast pressures, the mass of air involved is comparable to the mass of explosive. Consequently, the shape, detonation mode, and other details of the chemical explosive have persistent influences on the blast wave and fireball, and prevent rigorous adherence to the conditions for the simple atmospheric scaling suggested above.

For nuclear explosions, however, the energy density is so high that the mass of the source becomes negligible long before the blast wave has become weak, and the early fireball growth by radiation transport provides a scalable effective source so long as the air temperature at which the shock begins to form is about the same. Even when it is not the same, the deceleration of the radiative growth is so sharp a function of the radius that the initial effective fireball begins driving the shock with nearly the same energy per unit volume and at a nearly Sachs-scaled radius.

When the nuclear burst occurs at a high enough altitude that the radiative growth is substantially different, then the simple scaling is invalid. The longer mean free paths at high altitude allow the fireball to grow to a larger radius and lower temperature before slowing enough for a shock wave to form.

Fireball—After Shock Breakaway

At a time of about 80 msec for this example of 1 MT at sea level, the shock wave has expanded and weakened to such an extent that the shock temperature is relatively low, of the order of 2000°, at which temperature air is no longer strongly luminous. For this reason, we begin to see through the shock front into the hotter interior. Subsequently, as the fireball continues to expand and the density continues to drop in the interior, the temperature to which we can see rises and the intensity of thermal radiation rises appropriately. Although the shock wave continues to expand, eventually the hot interior region which is the late fireball slows and finally ceases to grow. The shock wave by then has become separated and quite independent of this late fireball.

Figure 9 illustrates the temperature profiles that would be typical of a 1-MT sea level explosion in this late time period. As the thermal radiation

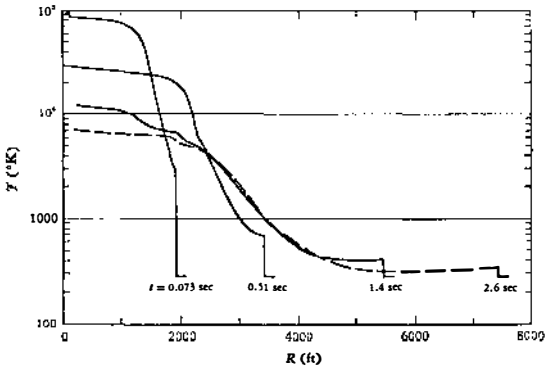

FIG. 9. Late fireball temperature versus radius (1 MT-surface burst).

depletes the energies of the fireball interior at the times approaching a second, the temperatures in the interior drop markedly to temperatures of the order of five or six thousand degrees, below which the radiation rate is extremely slow.

The corresponding late-time densities are illustrated in Figure 10. The gradual slowing down and depletion or the dissipation of the fireball itself is again evident in the extent of low-density air. At times of several seconds a low-density sphere (of modestly high temperatures) is left, which then further cools mostly by rising and mixing in the atmosphere. Of course, at these late times, beyond the time of the maximum intensity in thermal radiation, one can expect to see completely through the system of shock waves and fireball air and to see, then, the bomb vapors themselves.

Figure 11 indicates something of this late-time fireball temperature structure for this 1-MT example at 1.3 sec.

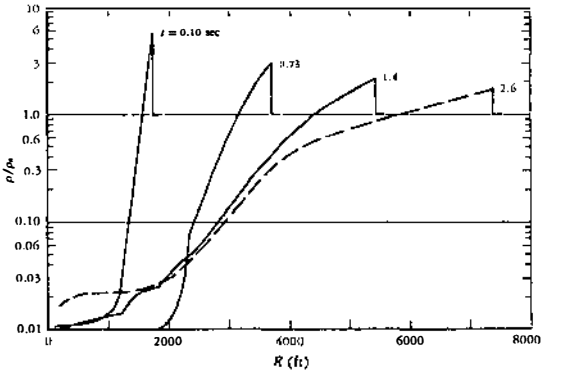

FIG. 10. Late fireball densities versus radius (1 MT-surface burst).

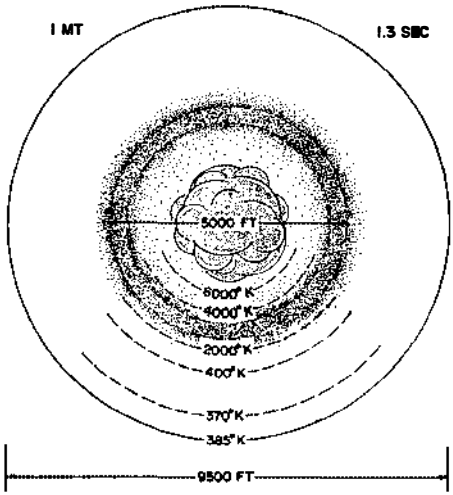

FIG. 11. Late shock and fireball size and temperature.

Figure 12 illustrates the temperature history within and close to the fireball. The different curves are characterized by the peak overpressure of the shock at those distances for this 1-MT example. For instance, the 100-psi point is at a distance from the point of burst of approximately 850 m. Whereas this 100-psi point is about at the edge of fireball, the 40-psi distance (1500 m) is clearly outside the fireball, and it experiences a far less severe temperature history. The 200-psi point, at a distance of about 640 m, experiences temperatures in the thousands of degrees for a matter of several seconds. For such a fixed point on the ground or above it, the temperature

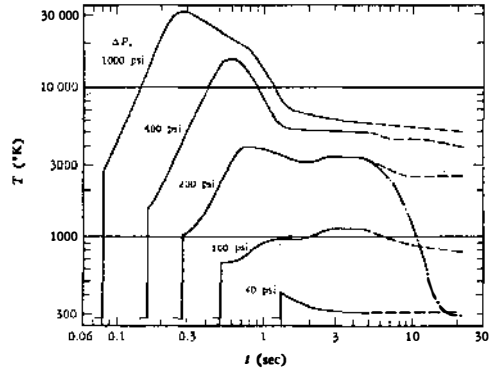

FIG. 12. Temperature versus time at high peak overpressures 1 (MT-surface burst).

ultimately drops back to normal as the fireball rises away from it in the atmosphere. Most of the rise occurs after the shock wave and the thermal radiation have played out their roles in the fireball development. The dashed curve which drops from the 200-psi curve indicates the nature of this temperature drop due to such fireball rise. The other curves show a continued high temperature, but do not at these late times represent reality, even within the rising fireball. The calculations of this kind which provided these numbers (2) do not include any of the cooling due to mixing, rising, and expanding in the atmosphere, all of which are important in the late fireball dissipation.

Although these temperatures at very close-in distances are indeed impressive, the response of materials for such a relatively short exposure is by no means simple, and can by the use of straightforward thermal diffusion predictions be much exaggerated. The dynamics of the surface interactions is such as to provide considerable protection against ablation for relatively long times.

Figure 13 illustrates an interesting feature in the fireball growth: the continued effect of radiation diffusion even after a shock wave is formed at the fireball front. Here is a Lagrangian plot (a plot following the history of certain air particles) versus time for air particles that were shocked to temperatures of 40000 to 20000 and to 10000 degrees. After the shock arrival (which is the sharp rise) the air particles begin to cool in the expansion behind the shock, but at a later time these particular air masses are overtaken by the advancing radiation diffusion front and are then reheated even while continuing to expand behind the shock wave. This effect decreases rapidly, so that out in that air which is struck by a 10000° shock, there is relatively little subsequent heating due to any continued radiation diffusion.

Most of these considerations have been in the absence of a number of features that are frequently important if not dominant in determining the

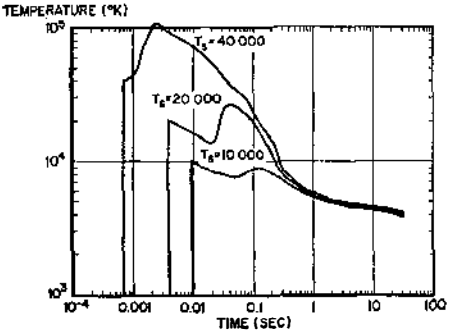

FIG. 13. Temperature histories of air particles shocked to 40 000, 20 000, and 10 000° K showing effect of continued radiation diffusion after shock formation.

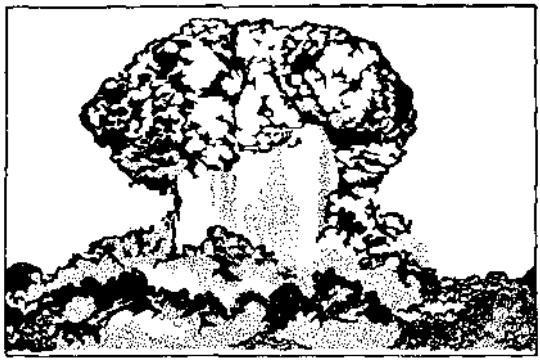

FIG. 14. Turbulent mixing from late fireball or early cloud.

character and the phenomena of the fireball. Figure 14 illustrates some of these imperfections or some of these complicating features when an explosion takes place close to other materials, as in a surface burst. It is possible that large quantities, indeed—for a surface burst, literally megatons of earth material (for megatons of explosion yield)—become involved in the fireball gases at a very early stage. That is, much of the cratered material is thrown up into (and intimately mixed with) the fireball before its thermal radiation maximum is reached. Such large amounts of material must considerably influence the nature and the timing of the subsequent thermal radiation, and the total amount of radiation. It does, of course, have a marked effect on the fireball, as evidenced by high-speed pictures. The fireballs are by no means spheres nor are they rigorously even segments of spheres; there are frequently perturbations of precursor-type shock waves on or near the surface which further obscure a portion of the fireball. Numerous reflected shocks are transmitted back through the fireball, which further change its state (Figure 15). In the latest time periods the vast amounts of debris so entrain the energy, and provide such an increase in the opacities, that the rate of radiation may be determined by the rates at which the hot gases are brought to the surfaces of turbulent vortices rather than by any radiation transport rates. The complicated state of affairs for such surface and near surface bursts in the late stages is suggested in Figure 14.

FIREBALL—ALTITUDE EFFECTS

Consider the effect of the atmospheric density on the fireball. The equation of state of air has a specific heat at high temperatures which increases somewhat as one goes to lower densities, i.e., to higher altitudes. More important are the changes in the optical properties of the air with varying ambient density. Low density leads to longer mean free paths or lower ab-

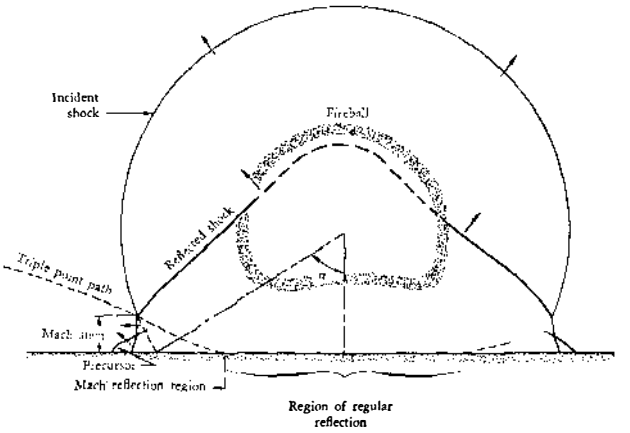

FIG. 15. Shock configurations (low air burst).

sorption coefficients and allows radiation flow to dominate more of the fireball history.

Figure 16 illustrates something of the change in the equation of state. It shows the ratio of pressure to energy per unit volume as a function of the air temperature for various air densities relative to sea level air [from air ten times normal density to one millionth of normal density (6)]. The salient feature of this set of curves is that at very low densities, and in some temperature ranges, the pressure can be very low while the energy per unit volume remains high. In fact, for low densities this ratio can become less than half of what it is for sea level air at temperatures around 10000°. Such temperatures are critical to the fireball since this is a temperature characteristic of the period in which much of the thermal radiation is emitted.

This disparity in the relation between pressures, temperatures, and energies is likely to result in some differences in the blast wave and, there-

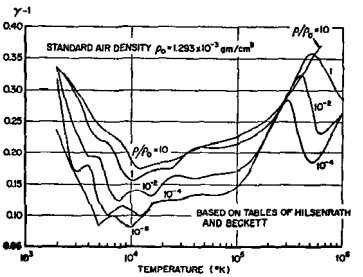

FIG. 16. Pressure-energy parameter, $\gamma\text{-}1 = P/\rho E$, for air at various densities, as a function of temperature.

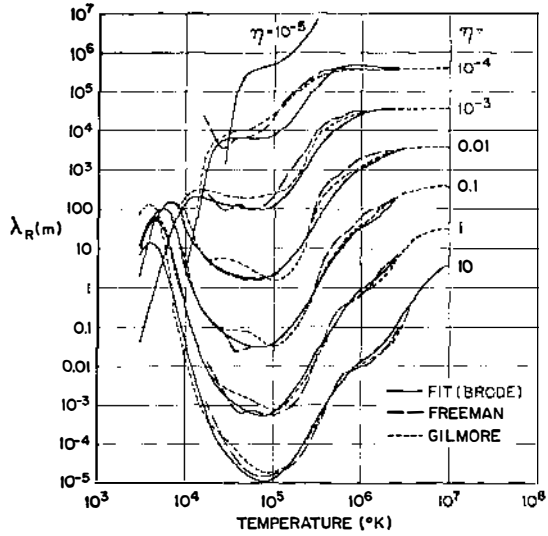

FIG. 17. Rosseland mean free path for air—used in radiation diffusion calculations ($\eta = \rho/\rho_0$).

fore, in the rate of expansion of fireballs; but a more serious change in the properties of fireballs is characterized by the changes in optical properties with air density changes. One such indication is illustrated in Figure 17, which shows curves of the Rosseland mean free path for radiation in air as a function of temperature for a similar range of densities (7, 8). Here, it is evident that over much of the temperature history of the fireball at sea level (where densities at the front or in the shocks are greater than that at sea level), the mean free paths are often as short as a few centimeters to even fractions of a millimeter. In any case, at sea level the mean free paths are much shorter than fireball dimensions at temperatures below a million degrees. On the other hand, for high-altitude explosions, where the densities are small fractions of the sea level density, the mean free paths may become everywhere long and indeed eventually can become much greater than the size of the fireball itself. In such cases, fireballs begin to disappear altogether, leaving only the bare bomb vapors to expand and radiate.

THERMAL RADIATION

The earliest radiations from the fireball in the visible and infrared are complex and diffuse and relatively weak. One might expect, on the basis of a simple blackbody spherical radiator model, to find that the most intense light occurred as the radiation first flooded out of the bomb materials and that as the fireball grew, the intensity decreased monotonically. For such a model the power radiated can be expressed as

$$P = 4\pi R_s^2 \sigma T_s^4 \quad \text{ergs/sec} \qquad 25.$$

in which the fireball surface area is $4\pi R_s^2$ and σT_s^4 is the blackbody radiation rate [the Stefan-Boltzman constant $\sigma = 5.6687 \times 10^{-5}$ ergs/cm^2/sec/(°K)^4]. This simple form agrees quite well with observed thermal power *after* the first maximum and before the minimum in the light intensity. It does not apply in the earliest phase because the fireball is far from a blackbody. It is surrounded by air whose transparency to visible light is altered by the X rays and to some extent by the gamma rays and neutrons. Until the fireball can expand and engulf the veil of disturbed air, its high-temperature surface cannot be seen clearly at a distance, and its first thermal maximum has not been reached.

If the fireball were an isothermal ideal gas, then the temperature (like the specific energy) would decrease linearly with increasing volume, or as the inverse cube of the radius. In fact, since the hot air has a great deal more specific heat than when it is cold, and since the fireball is far from isothermal during the early shock expansion (temperature rising steeply behind the front), the fireball front or shock front temperature decreases more nearly as the inverse square of the shock radius for much of its expansion. If such a proportionality is included in Equation 25, then the thermal radiation power should decrease as about the inverse sixth power of the shock radius. Since the strong shock behavior suggests a shock radius increase proportional to the two-fifth power of the time, the thermal power should decrease about as the inverse 2.4 power of the time. While this behavior should apply to the time after first maximum and before minimum, it is necessary to further modify Equation 25 for comparison with observations at a distance. During this time, the effective radiating temperatures may be as high as 1 or 2 eV (10 000-20 000° K), so that a large fraction of the blackbody spectrum will lie in the ultraviolet, at shorter wavelengths than the visible, and the atmosphere will not pass such light. In fact, much of it will be absorbed in the immediate vicinity of the hot fireball surface. This ultraviolet cutoff is quite sharp at 1860 Å for oxygen, and if one integrates the Planck spectrum with such a cutoff, a function of temperature $f(T)$ results (9) such that at high blackbody temperatures (where only the tail of the spectrum is allowed to radiate) the effective radiation rate $\sigma T^4 f(T)$ becomes proportional to T. At low temperatures $f(T) \sim 1$, and the full blackbody rate can escape. An analytic approximation to this cutoff function for 1860 Å is as follows:

$$f(\phi, 1860\ \text{Å}) = 25/(25 + 4.7\phi^3 + 1.6\phi^8) \qquad 26.$$

in which the temperature (ϕ) is in electron volts.

While radiation of wavelength longer than 1860 Å can escape the fireball, some of it is still rather readily absorbed, and only that fraction that lies beyond about 3500 Å (the ozone cutoff) is observed at large distances. Figure 18 shows the cutoff function versus temperature for cutoffs at 1860 and 3500 Å. Also shown are $T^4 f(T)$ for these cases.

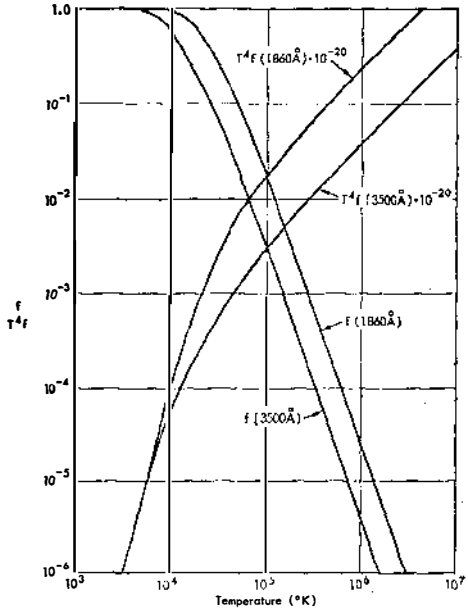

FIG. 18. Blackbody cutoff function (f) and T^4f versus temperature for cutoffs at 3500 and 1860 Å.

When the expanding shock cools below a few thousand degrees, its emissivity falls, it becomes transparent, and the hotter air behind it shines through. At such a time, the shock wave appears to separate from the fireball, the fireball brightens but slows in its expansion, and the shock races away. Because higher-temperature air is exposed, and the fireball radius is still growing, the rate of radiation increases rapidly until the hottest interior air is exposed and begins to cool. This constitutes the rise from light minimum to second maximum in the thermal pulse.

Figure 19 illustrates something of the nature of this increasing optical depth concept. It shows the local-emission mean free path[4] as a function of

[4] The emission or Planck mean free path is defined as the following example:

$$\frac{1}{\lambda_P} = \int_0^\infty \frac{1}{\lambda_\nu} B_\nu d\nu \Big/ \int_0^\infty B\nu d\nu$$

where λ_ν is the frequency-dependent emission mean free path, and B_ν is the blackbody radiation intensity, such that $B \sim T^3(u^3/e^u-1)$, $u = h\nu/kt$. Such an average emphasizes the contributions where the frequency-dependent emission mean free path is shortest. In contrast, the Rosseland mean free path (appropriate in the diffusion approximation) is defined by the average

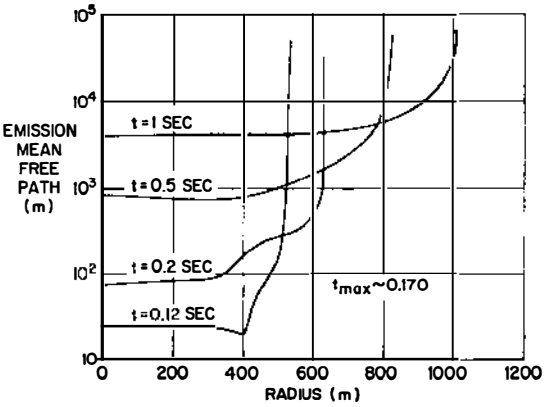

FIG. 19. Planck (emission) mean free path versus radius at various times for 200 KT, 60 Kft.

radius for a 200-KT fireball at 60 000 ft burst altitude at various times shortly before and after the time of maximum thermal power output. The earliest curve (at 0.12 sec) shows that mean free paths are nearly everywhere much shorter than the radius of the fireball itself. At two tenths of a second, the mean free paths in the hot region are becoming comparable to the dimensions of that hot region, and are already larger than that region out in the cooler exterior air. At a half a second for this 200-KT example, emission mean free paths are everywhere nearly a kilometer in length, while the fireball is smaller. In other words, the fireball is already nearly transparent, and its rate of radiation or emission decreasing.

In a megaton explosion there is a greater thickness of shocked air and so more mean free paths for absorption of the radiation from the hot interior than exist in a kiloton explosion at the similar stage in its history. It should follow that more expansion and cooling and greater transparency (lower emissivity) will be required in the larger explosion before a comparable fraction of the inner heat can be released. This suggests a scaling of thermal phenomena that takes longer than the blast scaling would indicate. The following empirical scaling rules show such a trend.

Thermal pulse scaling

time to first maximum $\simeq W^{1/3}\eta^{\circ}$ msec 27.

time to minimum $\simeq 60W^{0.40}\eta^{\circ} \pm 35$ per cent msec 28.

time to second maximum $\simeq 0.90W^{0.42}\eta^{0.42} \pm 20$ per cent sec 29.

$$\lambda_R = \int_0^{\infty} \lambda_\nu \frac{dB_\nu}{dT} d\nu \Big/ \int_0^{\infty} \frac{dB_\nu}{dT} d\nu$$

which emphasizes spectral contributions where mean free paths are largest.

$$\text{power at second maximum} \simeq 1.2^{+15} W^{.6} \eta^{-.42} \text{ watts} \tag{30.}$$

$$\text{thermal yield/total yield} \simeq .4 + \frac{0.06 W^{1/2}}{1 + 0.5 W^{1/2}} \tag{31.}$$

$$\text{visible light yield/total yield} \simeq .27 + .06\eta \frac{.12 W^{1/2}}{1 + W^{1/2}} + \frac{114\eta}{8200\eta^2 + 1} \tag{32.}$$

where W is the yield in MT.

Nuclear Radiation

Although the initial nuclear reactions (responsible for the energy generation in a nuclear explosion) take place largely inside the bomb and are over in a fraction of a microsecond, some nuclear radiations persist for long periods after the burst and are scattered or radiated from atoms far outside, as well as inside, the bomb debris. Approximately 90 per cent of the neutrons generated are absorbed within the bomb, but the remaining fraction that escapes creates impressive doses in the air. An even larger percentage of the gamma rays emitted during the fission process are absorbed in the bomb, but gamma rays coming from the excited fission-fragment nuclei continue to radiate for a long time. Gamma rays further result from neutron capture in nitrogen—a capture leading to the emission of gamma rays in about 6 cases out of 100.

A bomb may be viewed as the source of a neutron flux roughly proportional to the energy release or yield. The neutron flux (neutrons per unit area, e.g., n/cm^2) must decrease at least as rapidly as the inverse square of the distance from the explosion source, since the total number of neutrons passing through a spherical surface at any distance does not increase and since the area of the surface increases as the square of the radius. In addition, the flux will be reduced by the removal of neutrons absorbed in the air along the way; and since the number *absorbed* in any distance is nearly proportional to the number *reaching* any distance, an exponential decay in the flux with increasing distance from the point of burst is expected:

$$N(n/\text{cm}^2) \simeq \frac{2^{+22} W_{mt}}{R_{ft}^2} \exp\left[-(R\rho/780)\right] \tag{33.}$$

where ρ is the density of air in grams per liter ($\sim$1.1 for average sea level conditions).

When converted to units of rads,[5] this formula becomes

$$N = \frac{5^{+13} W_{mt}}{R_{ft}^2} \exp\left[-(R\rho/780)\right] \text{ rads} \tag{34.}$$

[5] For typical neutron spectra from nuclear explosions, n/cm^2 is approximately related to units of radiation absorption by the following conversion: 4.4×10^8 n/cm^2 $\simeq$1 rad, where the rad is defined as the amount of radiation (neutrons) which will produce 100 ergs of absorbed energy per gram of soft tissue. Of the various measures of nuclear radiation intensity, the roentgen unit for gamma rays and the rad for neutrons will be used here. The roentgen represents gamma rays of such intensity that 87 ergs are absorbed in 1 g of air, but in soft tissue (meat) the same intensity deposits about 97 ergs per g, or nearly 1 rad.

The source of gamma rays, being in part dependent on neutron captures as well as on fission-fragment decays, is a more complicated function of both time and space. The fission-fragment radiation decreases with time in proportion to approximately the inverse 1.2 power of time, while the capture gammas are nearly all generated in the first 1/100 sec. Although gamma rays traverse the air with roughly the same kind of geometric divergence and absorption behavior as neutrons, the relatively long time for their emission allows the shock movement of the absorbing air to influence the dosage at distant points. This hydrodynamic effect can cause large increases in the gamma-ray dose over the dose that could be expected in the absence of the expanding shock wave. But the effect cannot be important at the most close-in distances, where very little absorbing air lies between source and receiver before the blast. Neither can the effect amount to much at very great distances, where the air motions are both negligible and late. But at the intermediate ranges, where many mean free paths of air fill the intervening space (for 1-MT and greater explosions), and where shock motions are impressive, the hydrodynamic effect must be included in any analysis that aims to predict the levels of radiation even approximately.

Since the shock wave is nearly symmetrical about the bomb, it does not influence the spherical character of the gamma-ray flux, but it does change the character of the absorption and scattering (Figure 9). In a formulation similar to that describing the neutron flux, the hydrodynamic effect can be roughly included by allowing the mean free path (λ) and the effective amplitude of the source (α) to be functions of the yield:

$$D_\gamma = \frac{7^{+1\frac{1}{2}} W f \alpha \exp(-\rho R/\lambda)}{R^2}$$
$$\alpha = (1 + 6W^{\frac{2}{3}})/(1 + 0.03W^{\frac{2}{3}} + 0.005W^{\frac{4}{3}}) \qquad 35.$$
$$\lambda = 1070 + 1.5W^{\frac{2}{3}}$$

in which W is the yield in MT, f is the fission fraction (typically $\sim\frac{1}{2}$), and ρ is again the air density in grams per liter ($\sim$1.1 at sea level). This empirical formula matches most data to well within a factor of 2 for yields from 1 KT to 10 MT and from 1000 to 20 000 ft altitude of burst.

Properly, the dose is a more complex function of both yield and range, but over the above span of yields, and for radii corresponding to a few thousand feet, the formula above may suffice.

The table below (Table II) lists the relative gamma-ray and neutron doses, at some near distances from a 1-MT burst, together with the approximate overpressure level for surface bursts. When bursts are made at altitudes allowing greater coverage by blast and thermal, then the distances may be largely vertical, and effective air density will be less than that at the earth's surface. The table includes data for a range of effective ambient air densities to indicate the marked variation in doses from slight changes in meteorology or target and burst altitudes.

TABLE II

Prompt Dose Versus Distance

Range (miles)	Air density (g/liter)	1 KT			10 KT			100 KT			1 MT			10 MT		
		γ Rays (r)	Neutrons (rad)	ΔP_s (psi)	γ Rays (r)	Neutrons (rad)	ΔP_s (psi)	γ Rays (r)	Neutrons (rad)	ΔP_s (psi)	γ Rays (r)	Neutrons (rad)	ΔP_s (psi)	γ Rays (r)	Neutrons (rad)	ΔP_s (psi)
0.5	1.0	430	243		4300	2400		45 000	24 000		2 900 000	240 000		390 000 000	2 400 000	
	1.1	330	173	1.6	3300	1700	~6.3	35 000	17 000	~32	2 300 000	170 000	~220	310 000 000	1 700 000	~1800
	1.3	200	88		2000	880		22 000	8 800		1 400 000	88 000		200 000 000	880 000	
1.0	1.0	9	2.1		90	21		960	210		62 000	2 100		11 000 000	21 000	
	1.1	5.5	1.0	0.5	55	11	~1.8	580	110	7	38 000	1 100	~37	7 200 000	11 000	~250
	1.3	2.1	.27		21	2.7		210	27		14 000	270		3 000 000	2 700	
1.5	1.0				3.4	.31		36	3.1		2 300	31		570 000	310	
	1.1	<1	<1	0.3	1.6	.11	0.9	17	1.1	3.4	1 100	11	~15	300 000	110	~85
	1.3				<1	—		3.9	.15		250	1.5		81 000	15	
2.0	1.0							1.7	.06		110	.59		37 000	5.9	
	1.1	—	—	0.2	—	—	0.6	<1	—	2	42	.15	~8	15 000	1.5	~40
	1.3										5.8	.01		2 700	.1	
2.5	1.0										6.1			2 700		
	1.1	—	—	0.13	—	—	0.4	—	—	1.4	1.8	—	~5	910	1	~25
	1.3										<1			100		
3.0	1.0													210		
	1.1	—	—	0.10	—	—	0.3	—	—	1.0	—	—	~4	58	—	~17
	1.3													4.4		
4.0	1.0													1.6		
	1.1	—	—	0.06	—	—	0.2	—	—	0.7	—	—	~2	<1	—	~9
	1.3															

The Electromagnetic Pulse (EMP)

The intense flux of gamma rays causes considerable ionization in the surrounding air out to several mean free paths. The electrons, being more mobile, are knocked outward at higher speed than the ions, and a sudden strong field is created by the charge separation. The Compton current is roughly proportional to the gamma-ray dose, the electron charge (e), and the ratio of electron pathlength (λ_e) to gamma-ray mean free path (λ_γ)

$$J \simeq \frac{e\lambda_e}{\lambda_\gamma} d_\gamma \left(t - \frac{R}{c}\right) \qquad 36.$$

where $d_\gamma(t - R/c)$ represents the gamma rays per unit area per unit time. (The dose given by Equation 35 is proportional to the time integral of d_γ.)

Unless the charge distribution develops some asymmetry, there can be no radiation field. Any burst near the earth's surface or with appreciable nonuniform masses associated with the explosive source is likely to radiate unevenly enough to produce charge asymmetries and an effective dipole radiator. The atmospheric density gradient is a minor source of asymmetry at sea level, but becomes more important at high altitudes where gamma-ray mean free paths become appreciable fractions of the atmosphere lapse rate. When a sufficiently large volume is ionized, as with a very high-altitude burst, the displacement of the earth's magnetic field can result in an appreciable electromagnetic pulse. Only when the burst is confined so that the gamma rays are absorbed in a small region (as underwater or underground) is the EMP likely to be absent or minimized.

The gamma-ray flux, expanding at the speed of light, rises in nanoseconds and continues (because of fission fragment nuclear decays) for a long time—decreasing somewhat faster than inversely with the time. The free electrons are quickly attached by atoms and molecules (with rates of 10^8/sec in sea level air) but the negative ions thus produced and the original positive ions last longer. Although much of the charge separation is canceled in milliseconds, the large ionized region that includes the growing fireball and its thermal ionization supports electromagnetic oscillations for many milliseconds. Within the first second the remaining fireball gases are mixing and turning vigorously and rushing through the atmosphere. From these and other causes, one may expect radiating electromagnetic signals (radio waves) from kilomegahertz down to fractions of a cycle per second or nearly direct current.

As with radar and uhf signals (megahertz to kilomegahertz) the high frequencies are more quickly attenuated in the atmosphere, but the propagation in the radio frequencies (kilohertz to megahertz) meets little absorption and, like lightning signals (spherics), can be detected around the world.

Within a few hundred kilometers, the signal is characterized by a continuous spectrum of median frequency around 10 to 15 kilohertz that is inversely related to yield (10). At much larger distances, the pulse is deter-

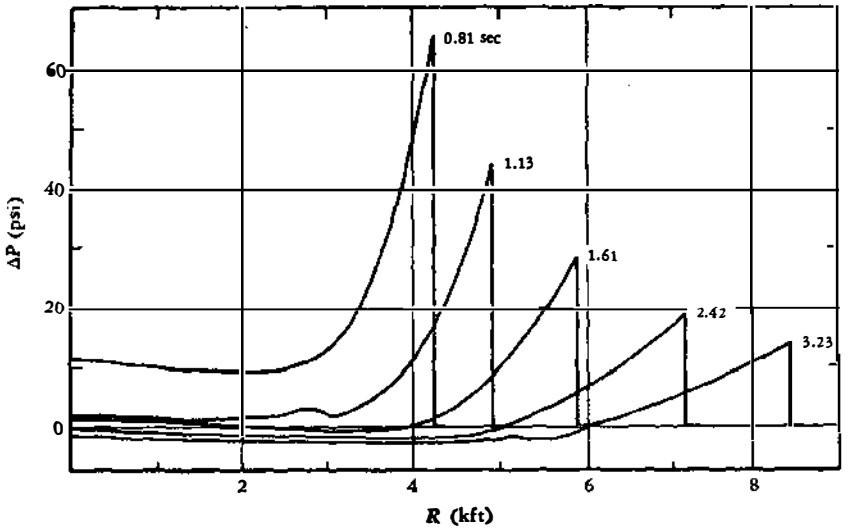

FIG. 20. Overpressure versus radius (1 MT-surface burst).

mined more by the properties of the atmospheric ducting (between the ground and the ionosphere), and thus is seldom distinguishable from natural spherics. Very close to a burst, the entire spectrum is present, and damage to both electrical and nonelectrical equipment can occur under the strong fields approaching tens of kilovolts per meter electric field, and hundreds of gauss of azimuthal magnetic field.

AIR BLAST

The pressure profiles of Figure 7 show typical strong shock, point source shapes, in that the pressure drops sharply behind the front to a nearly flat pressure in the fireball interior that is a half to a third of the shock pressure. This general behavior persists well beyond the strong shock region, but changes as the interior pressure reaches the exterior ambient pressure. Figure 20 shows the transition, as a negative phase develops. The negative overpressures (pressures below ambient) last for several seconds at a megaton, and fall as low as 3 psi (pounds per square inch) below ambient. Since that is more than 400 pounds/ft² of suction, the negative phase could pull open a blast door that is not designed to resist it. Figure 21 shows the shock arrival time and the shock radius as functions of the peak overpressure for a 1-MT surface burst. A good approximation to this peak overpressure versus distance relation is given by the expression

$$\Delta P_s = \frac{3300W}{r^3} + \frac{192W^{1/2}}{r^{3/2}} \text{ psi} \qquad 37.$$

with W in MT and r the range in thousands of feet (kft).

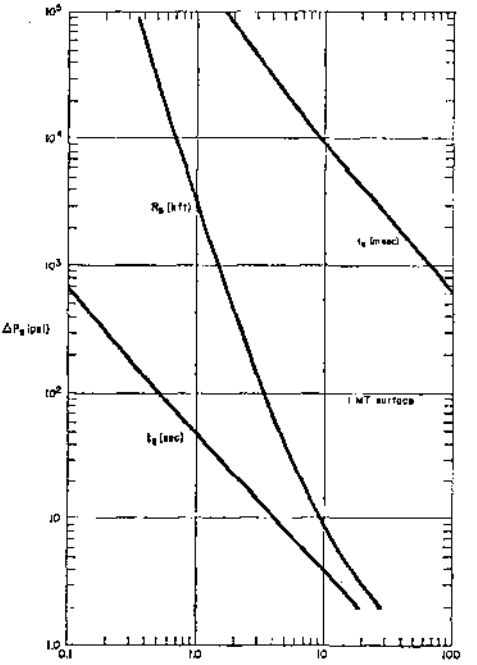

FIG. 21. Shock radius (R_s) and arrival time (t_s) versus peak overpressure for a 1-MT surface burst.

The initial decay of pressure behind the shock is extremely rapid at the higher overpressures, followed by a much slower exponential decay. The fast early decay comes from the passage of the spike, while the later decrease is characteristic of the fall of pressure on the inside of the blast wave. If time is measured from the instant of shock arrival, the blast pressures can be described as a sum of exponentially decreasing components.

$$\Delta P = \Delta P_s(1 - \tau)(ae^{-\alpha\tau} + be^{-\beta\tau} + ce^{-\gamma\tau}) \qquad 38.$$

with $\tau = (t - t_s)/D_P^+$ and D_P^+ being the duration of the positive phase (1 to 3 sec for a megaton surface burst), t_s the time of shock arrival, t the time, and ΔP_s the peak overpressure. The coefficients a, b, c, α, β, γ are given in Figure 22 along with the positive duration for 1 MT (surface burst), all as functions of the peak overpressure (ΔP_s). For other yields, only the duration need be scaled by the cube root of the ratio of the yield to 1 MT (by the cube root of the ratio of the yield to 2 MT for air bursts).

An alternative expression for the time dependence of overpressure takes advantage of the relatively simple relation between time and pressure when time is measured from the instant of the explosion. The product of pressure multiplied by the time is nearly a constant. Applying a 60 per cent correction

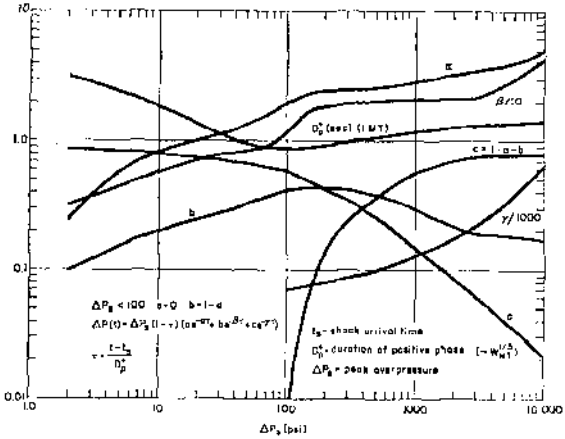

FIG. 22. Approximate analytic form for overpressure versus time for nuclear blast wave in terms of peak overpressure.

factor for the rapid decay behind the shock front leads to a form such as the following

$$\Delta P(t) = \frac{62}{1 + 13(t/W^{1/3})^{1.18}}\left[1 + 1.6\left(\frac{t_s}{t}\right)^6\right] \text{kb} \qquad 39.$$

with W in MT, and the time (t) and the arrival time (t_s) in milliseconds. A further approximation for the arrival time follows:

$$\begin{aligned} t_s &= 5.56^{-5}W^{1/3} + 5.8^{-19}R^{10}/W^3, \qquad \text{for } (R/W^{1/3}) \leq 44.4 \text{ m} \\ &= \frac{5.8^{-18}R^{10}}{W^3 + 3.6^{-14}R^{7.6}W^{1/3}} \qquad \text{for } 44.4 < R/W^{1/3} < 159 \text{ m} \\ &= 1.6^{-5}R^2R^{1/2}/W^{1/2} \qquad \text{for } R \geq 159W^{1/3} \text{ m} \end{aligned} \qquad 40.$$

At the earliest times (before a millisecond or so at 1 MT) and at the highest overpressure (>200 000 psi), neither form adequately describes the pressure history, since the shock is not well formed. The above formula (Equation 39) predicts too high a pressure close-in and too fast an initial decay above 200 000 psi. It also overestimates pressures (by a maximum of 20 per cent at 1500 psi) down to about 70 psi, below which it underestimates the overpressure (by as much as 20 per cent at 20 psi), becoming progressively worse. This latter form (Equations 39 and 40) is less exact than the previous fit (Equation 38) and is not valid at low overpressures. For some uses it is simpler, however.

Along with the high overpressures, the blast wave brings rapid air movements whose wind pressures (called dynamic pressure) can exceed the overpressure and cause much damage. The dynamic pressure is defined as kinetic energy density;

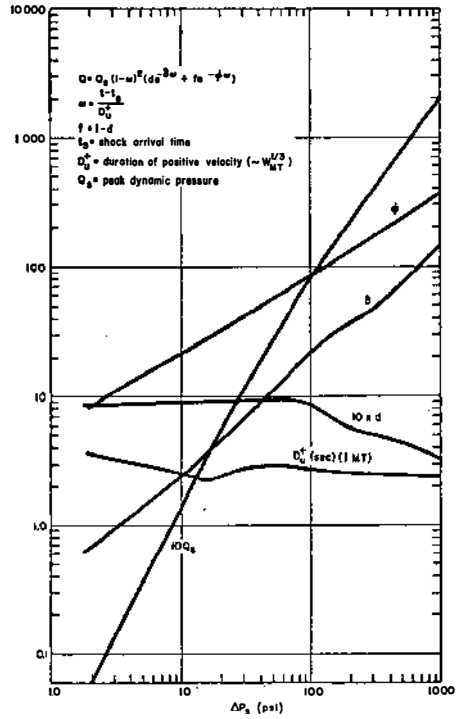

FIG. 23. Approximate analytic form for dynamic pressure versus time for nuclear blast wave in terms of peak overpressure.

[redacted] 41.

in which ρ is the air density and u the particle velocity.

In a form similar to that of Equation 38 for overpressure-time, Figure 23 gives the shock parameters and coefficients for obtaining the dynamic pressure variation with time

$$Q = Q_s(1-\omega)^2(de^{-\delta\omega} + fe^{-\phi\omega}) \qquad 42.$$

where

$$\omega = \frac{t - t_s}{D_u^+}$$

D_u^+ = duration of positive velocity ($\sim W_{MT}^{1/3}$)

Q_s = peak dynamic pressure

At 1000-psi overpressure, for example, $D_u^+ = 2.5$ sec and $Q_s = 2900$ psi; $d = 0.32$, $f = 0.68$; $\delta = 150$, $\phi = 350$; and $Q(t) = 2900\ (1-\omega)^2\ (0.32e^{-150\omega} + 0.68e^{-350\omega})$. The curve for Q in Figure 23 is in atmospheres.

Curves showing the pressure-time relations based on these analytic expressions are given in Figures 24 and 25.

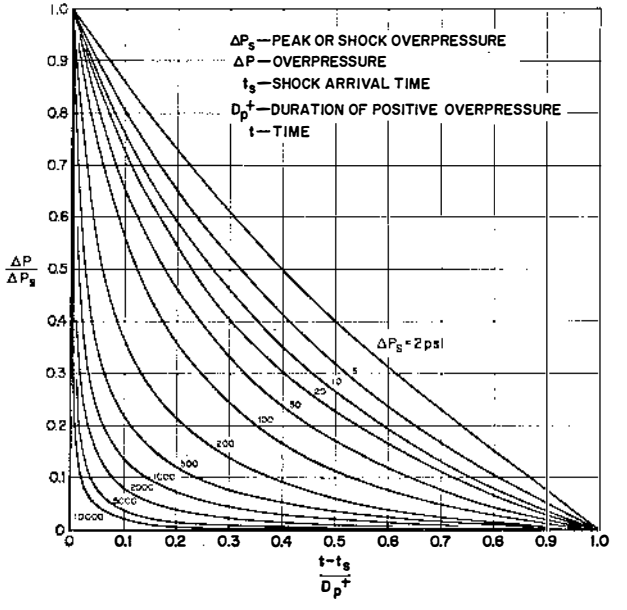

FIG. 24. Form factors for overpressures from nuclear explosions.

Some general features of an ideal or normal blast wave are illustrated as a function of the peak overpressure in Figure 26. Independent of weapon yield, the shock temperature, peak dynamic pressure, shock velocity, and maximum particle velocity at any point are related to the peak overpressure at that point as shown in this graph. The temperature and velocities increase with increasing peak overpressure, but they increase less rapidly than the peak overpressure itself. The peak dynamic or wind pressure rises very rapidly, however—more like the square of the peak overpressure at low overpressures—and is proportional to the overpressure itself only at the highest level.

The following analytical approximation for the shock velocity in terms of the peak overpressure (derived from the Hugoniot conditions for an ideal gas of $\gamma = 1.4$) is good to better than 8 per cent at sea level for all shock strengths.

$$U = C_0[.857(\Delta P_s + P_0)/P_0 + .143]^{1/2} \text{ ft/sec}$$

where C_0 (in ft/sec) is the ambient air sound speed and P_0 is the ambient air pressure.

The impulse of the blast wave is often a significant parameter in damage prediction; it is defined here as the time integral of the pressure taken over the duration of the positive phase. Figure 27 shows the general relation of the impulses for overpressure and dynamic pressure (along with the durations of each) to the peak overpressure. From this figure it can be determined that the

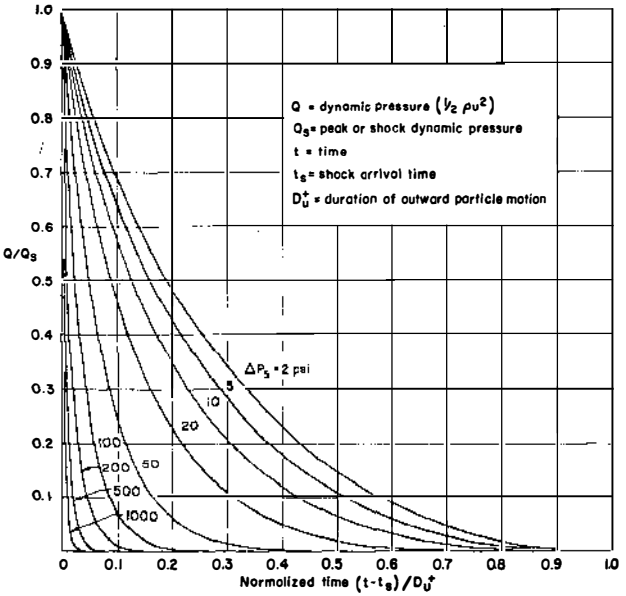

FIG. 25. Form factors for dynamic pressures from nuclear explosions.

overpressure impulse increases (with increasing overpressure) approximately as the square root of the overpressure below 1000 psi, and as the cube root at higher overpressures. Since at the higher overpressure levels the overpressure itself is proportional to the inverse cube of the radius, its impulse then is roughly proportional to the inverse radius. The dynamic pressure impulse decreases only very slowly with decreasing overpressure above 100 psi—being proportional in that region to about the fourth root of the overpressure—but it drops in importance very rapidly at lower overpressures. A good approximation for the overpressure impulse is

$$I_P{}^+ \simeq 1.83 \ (\Delta P_s)^{1/2} W^{1/3} [1 + .00385 \ (\Delta P_s)^{1/2}]$$

Although the total durations of the positive phase of overpressure and air velocity do not change greatly with overpressure, at the higher overpressures the bulk of the impulse is delivered largely in the first few milliseconds rather than uniformly over the whole positive phase. As illustrated previously in the pressure-time curves, the pulse shapes at high overpressures are much more peaked than at lower overpressures, and the exact duration of the positive phase is less important there than it is at the lowest overpressure levels (where the pulse becomes nearly linear in its time decay).

Figure 15 shows the shock after it has struck the ground beneath an air burst. A fused shock, called the *Mach stem*, is formed owing to the fact that

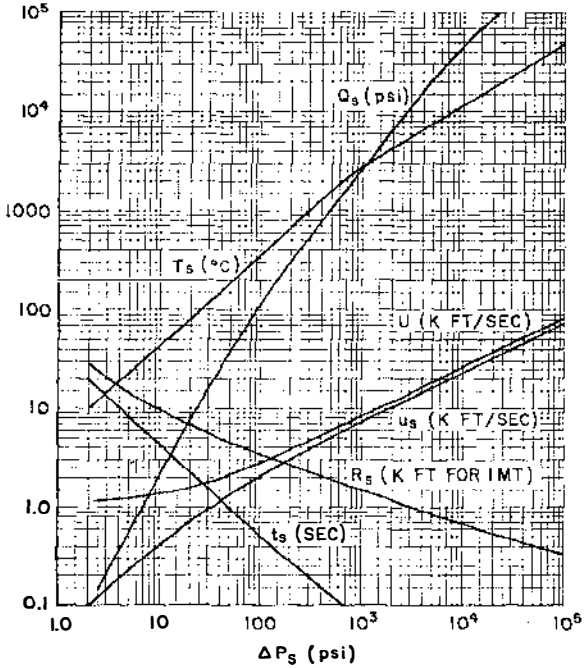

FIG. 26. Shock parameters versus shock overpressure.

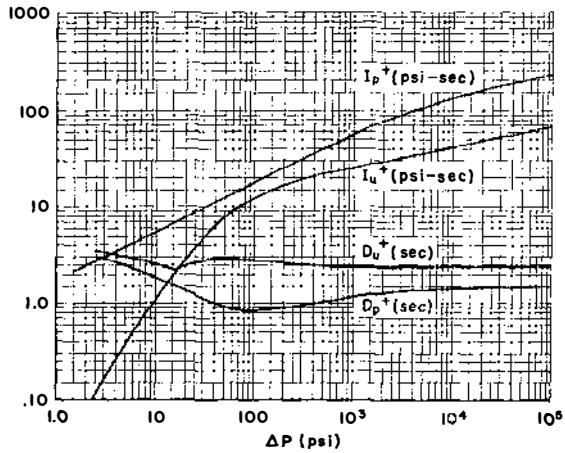

FIG. 27. 1-MT surface burst, impulses and durations in positive phase of overpressure and dynamic pressure.

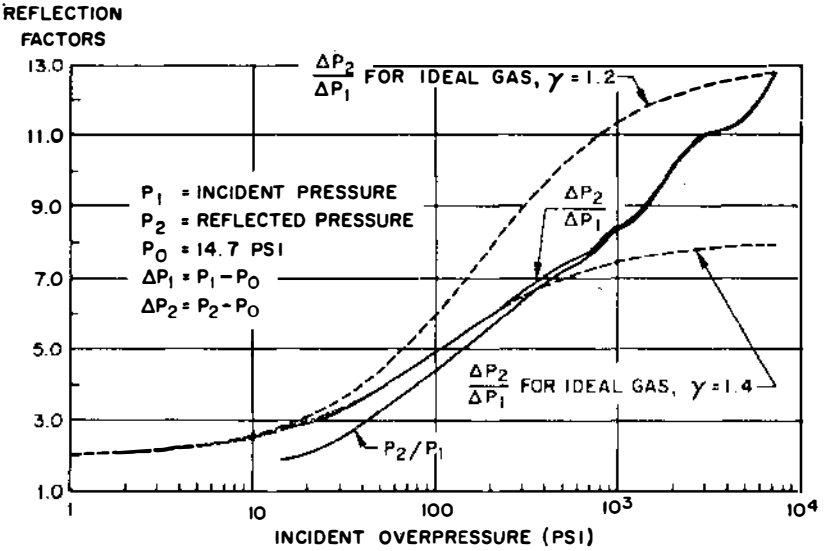

FIG. 28. Reflection factors for normal shocks—sea level air.

the reflected shock front, traveling through a region previously heated by the incident shock, overtakes the incident shock front and merges with it. The merged shock, or Mach stem, then travels nearly parallel to the ground surface. In this region ($\alpha > 45$ deg) the fused shock is stronger for the same slant distance, and its height increases gradually as the shock expands. The region of regular reflection (where the incident shock is followed by a reflected shock but is not overrun by it) also leads to overpressures much greater than the incident overpressure. Figure 15 also indicates some distortion of the Mach stem and precursor shock in front of it, both results of thermal radiation heating of the ground surface ahead of the shock. The pressure in such a precursed state does not have ideal properties but generally shows a slower rise to peak and a more irregular decay after maximum than are exhibited by normal shocks. For certain diffraction-type targets, such slow-rising pressures can greatly reduce the damage potential. For drag-type targets, the damage may actually increase because of precursed shock effects, since higher dynamic forces and greater irregularity in the duration and direction of destructive winds usually result.

When the shock front strikes an exposed surface normal to the shock ($\alpha = 0$), the overpressure is raised almost instantaneously to a reflected overpressure. Normally reflected shock pressures can be calculated and are given in Figure 28, which provides reflection factors versus initial peak overpressures. For a gas of a constant specific heat, characterized by a specific heat ratio $\gamma = 1 + PV/E$, the reflection factor can be written as

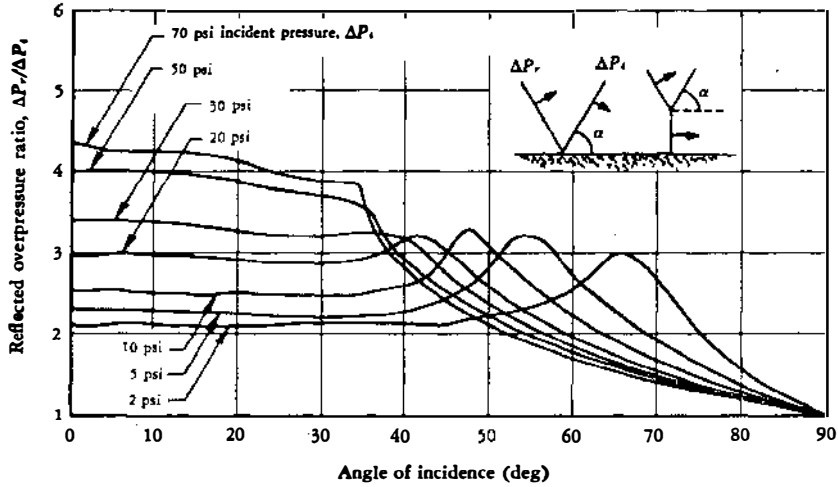

FIG. 29. Reflection factors versus incident angle and shock strength.

$$R = \frac{\Delta P_r}{\Delta P_s} = 2\frac{4\gamma P_0 + (3\gamma - 1)\Delta P_s}{2\gamma P_0 + (\gamma - 1)\Delta P_s} \qquad 43.$$

where P_0 is the ambient atmospheric pressure, ΔP_s the incident shock overpressure, and ΔP_r the reflected overpressure $(P_r - P_0)$. For shock less than about 50 psi in air, γ is very nearly 7/5, and the strong shock limit to the reflection factor is 8. But the effective gamma at high pressures is close to 6/5. Both are illustrated in Figure 28. Figure 29 gives values of reflected overpressures as a function of angles of incidence of the shock front and of the incident overpressure up to 70 psi. These curves demonstrate a trend toward a simpler reflection with less Mach-stem enhancement at increasing overpressures.

For closed rectangular structures, it has been found by shock-tube tests and by two-dimensional numerical calculations that the reflected pressure (ΔP_r) is reduced to the stagnation pressure at a time after shock arrival about equal to $3S/U$, where S equals the height or half the width of the structure (whichever is less) and U is the shock speed. The time $3S/U$ approximates the time required for the rarefaction waves, moving from the edges toward the center, to clear the front face of reflection effects.

The stagnation pressure is given by

$$P = \Delta P(t) + C_d Q(t) \qquad 44.$$

where C_d is a drag coefficient and may be of the order of unity for the front face of a structure and $Q(t)$, the dynamic pressure, is again $(\rho u^2/2)$, with ρ the mass per unit volume of the shocked and compressed air and u the free-

stream velocity of the air particles in the shock flow. For an ideal gas, the shock front dynamic pressure $Q_s(t)$ is approximated by the equation

$$Q_s = \frac{\Delta P_s^2}{2\gamma P_0 + (\gamma - 1)\Delta P_s} \qquad 45.$$

with γ ranging between 7/5 and 6/5 for air. For a standard sea level atmosphere the peak dynamic pressure is given graphically in Figure 26 as a function of the peak overpressure.

Air-Blast-Induced Ground Shock

A shallow-buried structure may be made quite safe from nuclear and thermal radiations and from the direct effects of air blast, so that the primary remaining vulnerability may be associated with the violent movements of the surrounding earth.

In addition to the intense direct shock in the ground that is responsible for the crater formation from a surface burst, ground motions are induced by the passage of air blast along the surface. For most surface or shallow-buried structures, this air-induced ground shock is of great significance since it is extended to large distances by the air blast, while the direct ground shock is more rapidly attenuated below damaging levels in passing through the intervening earth mass.

As long as the shock wave in air is strong and is moving at very high speed, the shock induced in the ground can only trail behind and below the air shock. In such a case, the ground shock can be conveniently characterized by the intensity and duration of the air blast passing nearly directly above. As the air shock slows and moves at a speed that falls below the speed of seismic signals in the earth, the motions generated in the ground may disperse. As a shock weakens, its velocity approaches the speed of sound in air. Seismic speeds in compact soil or rock generally are several times faster than sound speed in air, so the ground waves may move ahead as well as below and behind the air-shock position. The wave histories in this latter case are generally more complex and show greater variation from soil in homogeneities and stratifications.

One can at least derive some reassurance from the fact that the peak acceleration is less at depth and that some of the sharpness or higher-frequency components are missing at greater depths. This aspect points to a weakness in the applicability of elastic wave propagation theory. Dissipative mechanisms, either natural or artificial, can be extremely effective in reducing the peak stress or maximum velocity from such highly transient loads as those from air blast.

Some approximate formulas for predicting peak motions (acceleration, velocity, and displacement) near the surface are set forth below (11). Two sets of formulas are given, one where the air shock is superseismic (faster than the seismic velocities in the soil) and the other where the ground shock is "outrunning," i.e. can arrive before the air shock.

Superseismic Ground-Shock Maxima (at 5-ft depth)

Vertical acceleration:

$$\alpha_{vm} \simeq 340\, \Delta P_s / C_L \pm 30 \text{ per cent} \qquad 46.$$

Here acceleration is measured in grams and overpressure (ΔP_s) in pounds per square inch. An empirical refinement requires C_L to be defined as the seismic velocity (in feet per second) for rock, but as three fourths of the seismic velocity for soil.

Vertical velocity:

$$u_{vm} \simeq 75\, \Delta P_s / S C_L \text{ ft/sec} \pm 20 \text{ per cent} \qquad 47.$$

The specific gravity of the earth medium is denoted as S. In the following, the overpressure impulse (positive phase only) is designated as $I_P{}^+$.

Vertical displacement:

$$d_{vm} \simeq 20 I_p{}^+ (\Delta P_s)^{1/4} / S C_L \text{ ft} \pm 30 \text{ per cent} \qquad 48.$$

Since no attenuation is presumed, the stress is taken to be the same as the loading overpressure, but an exponential decay (as suggested in Equation 53) may be more reliable. A separate empirical approximation for maximum surface vertical displacement (upwards) near the crater shows a rapid decrease with increasing distance (R) beyond the crater (R_c)

$$d_{vm} \simeq .065 R_c{}^4 / R^3 \qquad 49.$$

Values of maximum horizontal displacement are likely to be half (or less) of the vertical maxima, while maximum horizontal acceleration and velocity are expected to be more nearly comparable to the vertical maximum values.

Outrunning Ground-Shock Maxima (at ~10-ft depth)

Vertical acceleration:

$$\alpha_{vm} \simeq \begin{matrix} 2 \times 10^5 / C_L r^2 \\ \end{matrix} \quad \begin{matrix} +\text{factor } 4 \\ -\text{factor } 2 \end{matrix} \qquad 50.$$

Acceleration is measured in g's, and r is the scaled radial distance—i.e., $r = R/W^{1/3}$ kft/(MT)$^{1/3}$.

Vertical velocity:

$$u_{vm} \simeq 4 \times 10^5 / S C_L r^2 \text{ ft/sec} \pm 50 \text{ per cent} \qquad 51.$$

Vertical displacement:

$$d_{vm} \simeq 6 \times 10^4 W^{1/3} S C_L r^2 \text{ ft} \qquad 52.$$

Horizontal motions in this outrunning phase may be quite comparable to the vertical movements.

Presenting these formulas in four examples, Table III shows some expected ranges of ground motion for 1 and 20 MT on soil of seismic velocity 4000 ft/sec, and specific gravity 2.

TABLE III

GROUND MOTIONS AT 5 TO 10 FT DEPTH IN 4000 FT/SEC SEISMIC VELOCITY SOIL (C_L=3000), AND SPECIFIC GRAVITY OF TWO (S=2)

Surface burst yield (MT)	One		Twenty	
Peak overpressure (psi)	50	500	50	500
Shock velocity (ft/sec)	2200	6100	2200	6100
Overpressure impulse (psi/sec)	13	40	35	110
Distance from burst (ft)	4500	1880	12 200	5100
Superseismic or outrunning	Out-running	Super-seismic	Out-running	Super-seismic
Maximum vertical acceleration (g)	2–13	40–74	2–13	40–74
Maximum vertical velocity (ft/sec)	1.6–5	5–7.4	1.6–5	5–7.5
Maximum vertical displacement (inch)	~6	5–10	~16	15–27
Maximum horizontal displacement (inch)	~6	2.5–5	~16	7.5–14

ATTENUATION WITH DEPTH

The attenuation of peak velocity with depth in the first few tens of feet of soil is largely due to dissipative losses and is not a strong function of weapon yield. Displacements decrease with depth both because soil is generally stiffer at depth and because vertical displacements approximately represent a sum of the decreasing strains beneath. Test data indicate (12) that after the rapid decay near the surface (to one half or one third of the surface motion), the maximum vertical displacement decreases further with depth according to the form

$$\delta = \delta_0 \exp(-.017D) \qquad 53.$$

in which D is the depth in feet and δ_0 is the shallow depth displacement. The effect of diverging geometry may be neglected for shallow-buried structures under loads from large yields, but can be an important factor in the decay of ground motions beneath low-yield explosions. To illustrate this geometry, Figure 30 shows the wave fronts in the air-induced ground shock. In the examples used, the earth media have siesmic velocities of 2500 and 5000 ft/sec, and fronts are shown at times when the peak air overpressures are 10 000, 1000, 300, and 100 psi. The curves represent positions achieved at uniform seismic velocities and take no account of faster ground-shock propagation at the highest stress levels or of variations in seismic velocity with depth. It is interesting that the effect of the rapid slowing of the air shock at around 300 psi (where it approaches the 5000-ft/sec seismic speed) results in a steep-

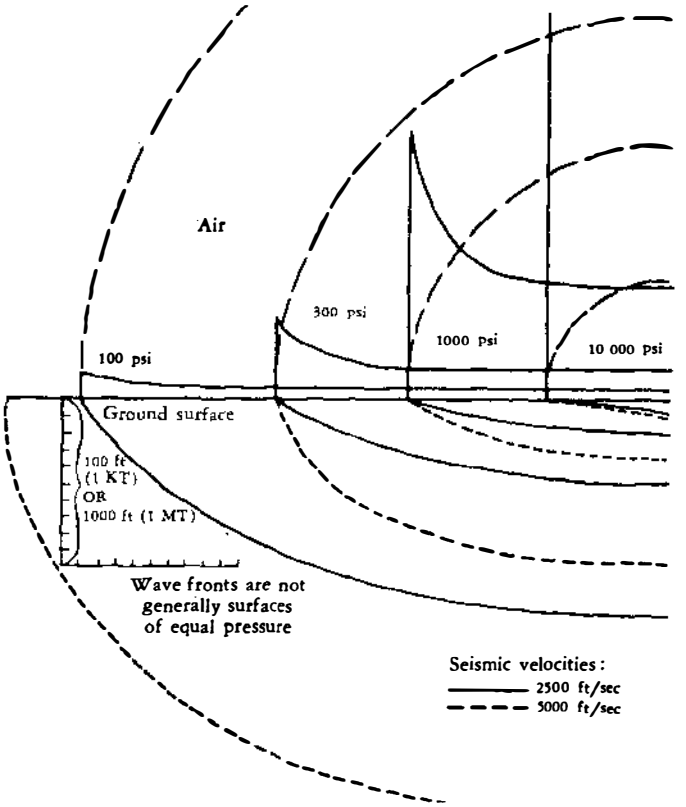

FIG. 30. Air-shock-induced ground motion wave fronts for peak overpressures of 10 000, 1000, 300, and 100 psi, and for seismic velocities of 2500 and 5000 ft/sec.

ening of the wave front and in a piling-up of the signal or waves from a considerable range of earlier shock positions. A similar condition is beginning at 100 psi for the slower seismic speed case (2500 ft/sec), but it is less pronounced since the air-shock speed is decreasing more gradually and so permits less of the ground wave to be superimposed. For the case of a 5000-ft/sec seismic velocity soil and an air shock at 100 psi (therefore traveling at less than 3000 ft/sec), clearly some signal in the soil can propagate ahead of the air shock, thus representing a region where one must expect ground-shock signals to arrive even before the air-blast arrival (the "outrunning" phase previously described).

It is obvious, but worth further emphasis, that the wave fronts of Figure 30 do *not* represent surfaces of equal pressure. In fact, the lack of spherical

divergence in the wave front directly below the point of burst would suggest that less geometric attenuation will occur there than in a more symmetric explosion. In the same vein, the ground shock just below the shock front at the 300-psi point for the 5000-ft/sec seismic speed case includes signals from pressures considerably higher than 300 psi and could, in that region, show ground stresses higher than the air overpressure.

It is equally certain that as we go to greater depths or to smaller yields—they are mainly the same thing since both depth and distance scale with the cube root of the yield—the spherical divergence of the shock energy into the below-ground space must further attenuate the shock strength.

Shock Spectra

Some information on the frequency characteristics of the ground shock is helpful, although for thorough analysis nothing short of full-time histories of the expected motions can be adequate. At high frequencies (greater than ~100 cps), the acceleration limits are most significant, since neither large amplitudes nor high velocities are likely to occur when the motions are reversing hundreds of times per second. At lowest frequencies, the displacements are of greatest concern. At fractions of a cycle per second (frequencies typical of earthquakes), the displacements can become a matter of several feet while accelerations remain less than 1 g and velocities are low.

Cratering and Direct Ground Shock

The crater that results from a nuclear detonation on hard rock has dimensions roughly 20 per cent smaller than those of a similar burst on soil or soft rock; i.e., a burst on rock excavates a crater volume only about one half that expected from a burst on soil. The efficiency of cratering by nuclear explosives depends on more than just the nature of the medium (hard rock, soft rock, dry soil, saturated soil, etc.); it varies also with depth of burst and with yield of the explosive, and is further sensitive to some details of the weapon and of its immediate surroundings at the instant of detonation.

The effect of depth of burst is particularly dramatic for nuclear explosives near the surface. The relatively small mass and physical dimensions of a nuclear charge (in comparison with the mass and size of its high-explosive equivalent) make the crater from a low air burst or contact burst much less impressive, while for an adequately buried and tamped nuclear charge, the surrounding earth in large part compensates for the disparity in explosive mass and size. The dependence of crater radius and crater depth on depth of burial of a 1-KT nuclear charge is illustrated in Figure 31. Some typical data points are included. The sharp change in crater efficiency at the exact surface of the earth is only slightly exaggerated.

Crater dimensions may be approximately scaled for other-yield weapons by multiplying depth by the fourth root of the yield ($W^{0.25}$) and diameter by the yield to the three-tenths power ($W^{0.30}$). Such an empirical scaling is

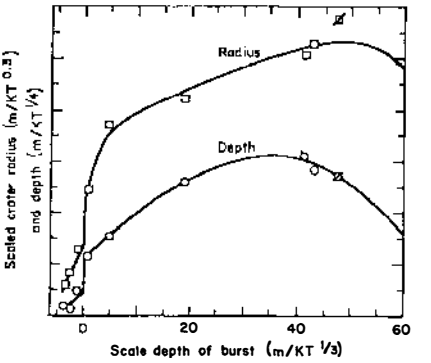

FIG. 31. Crater dimensions versus depth of burst (1 KT).

used in Figure 32 to approximate crater dimensions for three types of bursts in hard rock: for surface or contact bursts, for shallow-buried bursts, and for bursts buried deep enough to maximize the crater volume.

Theoretical work in recent years has contributed considerably to an understanding of the cratering action of nuclear explosives. Viewed in axial symmetry, the early soil dynamics has been modeled with two-dimensional hydrodynamic and elastoplastic numerical methods. Such models are still far from complete. The use of hydrodynamics is strictly justifiable only in that region where the ground medium is subject to stress well in excess of its shear strength, while final crater dimensions are likely to be influenced as much by the subsequent lesser stresses and motions characteristic of solids under compression and shear. On the other hand, solid-state properties and

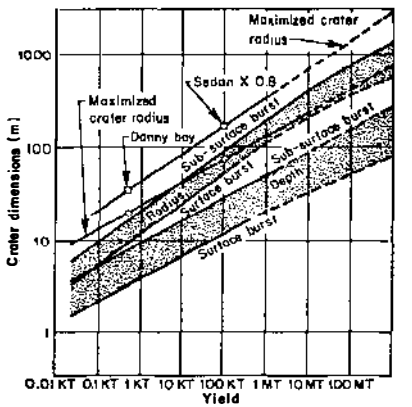

FIG. 32. Crater scaling.

complete models for natural materials are seldom available in forms appropriate for use in numerical calculation.

The extremely high energy densities and temperatures of a nuclear explosion guarantee the validity of a hydrodynamic treatment in studying close-in soil response, since the initial strong shock will vaporize the earth for some distance. Because the geometry of the burst relative to the interface separating ground and air strongly influences the formation of a crater, a hydrodynamic model in two dimensions, including vertical and radial motions, is vital to a description of pressures and velocities during and following crater formation.

Although such a calculation may include the effects of both the high pressures of the bomb-vapor residual energies and the pressure or impulse from the air-blast slap, early results (13) have shown that the extremely high-pressure impact of the bomb material itself is most important in the excavation process. The air slap does indeed send a shock into the ground, but it is over a wide area and at pressures several orders of magnitude less than those in the direct shock out of the bomb. While the air blast is born in a great fireball, which begins pushing on an area many times that of the eventual crater, the remaining energy in the bomb vapors is so concentrated as to vaporize and eject quite forcefully the immediately surrounding material. Out along the surface beyond the region of the crater, the air-blast slap will induce ground stress that will exceed any stress directly propagated that far from the initially intense bomb shock (which arrives later); but for the cratering action, and for shocks immediately below the crater, the effect of air slap is truly negligible.

Thus the internal and kinetic energies delivered directly to the ground from the bomb are most important in forming a near-surface crater and inducing ground motion below it. For this reason, the precise height or depth of burst and the details of the bomb disassembly have an important influence on the crater and on the energy initially delivered into the soil. Shallow burial and denser bomb cases may enhance the cratering efficiency by very significant factors.

A true contact burst might be expected to deliver half its momentum downward into the soil and half upward into the air. However, only a fraction of the bomb energy finds its way into kinetic motion of the bomb materials. Further, since the soil is at least a thousand times denser than the air, the dynamics of a surface burst require for conservation of momentum that the velocities imparted to the soil be less than those created in the air by just this ratio of densities. The kinetic energy imparted in this way will be proportional to the square of the velocity, and so will be proportionately much less in the dense material. In one example, something like 15 per cent of the energy from a 1-MT surface explosion started out into the ground (13).

Figure 33 illustrates the pressure contours typical of a surface burst of a few megatons on a relatively soft volcanic rock material at about 1/10 msec after detonation. Pressures are in kilobars (kb), so that the pressures shown

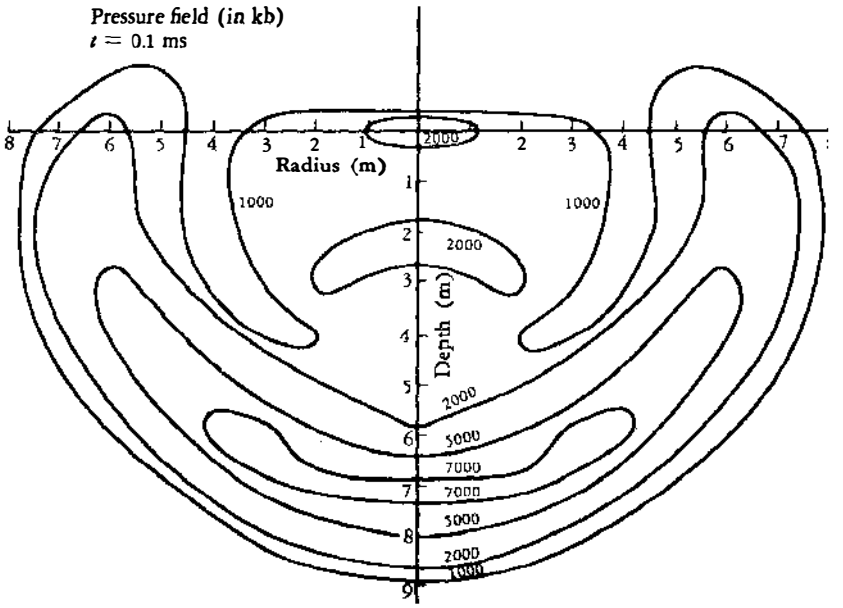

FIG. 33. Earth pressure contours from surface burst ($t = 0.1$ ms).

run to several megabars (Mb). The early response is centered in a downward hemispherical shock several meters below the burst point. The presence of the surface has already caused some relief of pressure at shallow depths, but the main shock appears to be fairly uniform and spherically diverging in a vertical cone about 90 degrees in width.

Figure 34 illustrates a velocity field at this same early time, with the same portion of a spherical shock appearing. Rock vapor is already streaming upward at velocities of several tens of meters per millisecond.

At a time of some 50 msec, a relatively late time in the cratering action, the pressure contours still show much the same curved shock with continued surface relief (Figure 35). The shock strength is now down to about 7 kb at a depth of 160 m, and pressures are perhaps beyond a level where hydrodynamics should give way to consideration of the solid-state properties of the rock—the medium no longer being a true fluid. Crushing, plastic, and viscoelastic behavior could be expected to have important influences both on the subsequent wave propagation and on the response of an imbedded structure. In this analysis, the portion of the shock running vertically below the burst point remains the strongest; and it may represent a significant limitation to the survivability of structures directly underneath a large-yield explosion.

The velocities at this time (Figure 36) show a rather clear division of

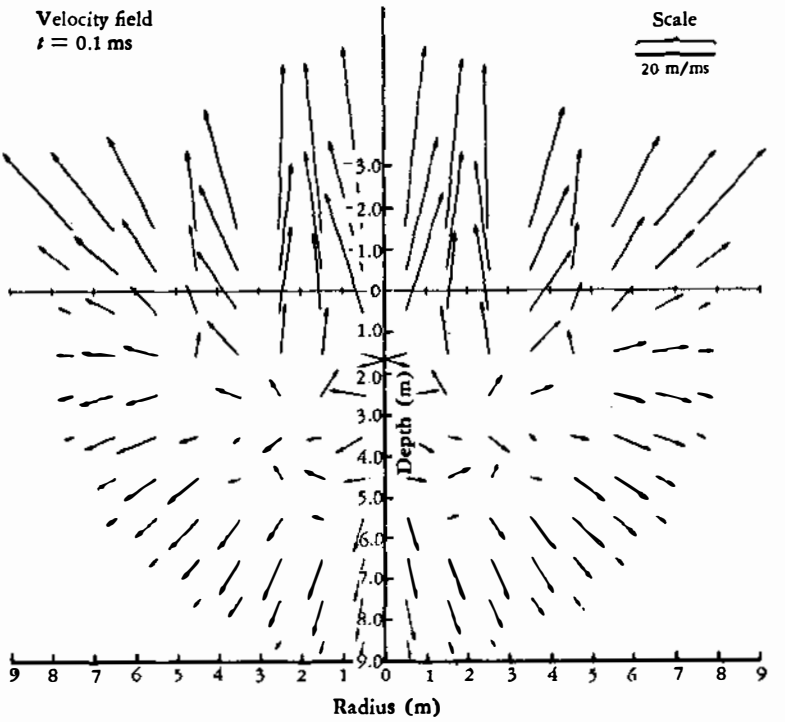

FIG. 34. Particle velocities from surface burst ($t = 0.1$ ms).

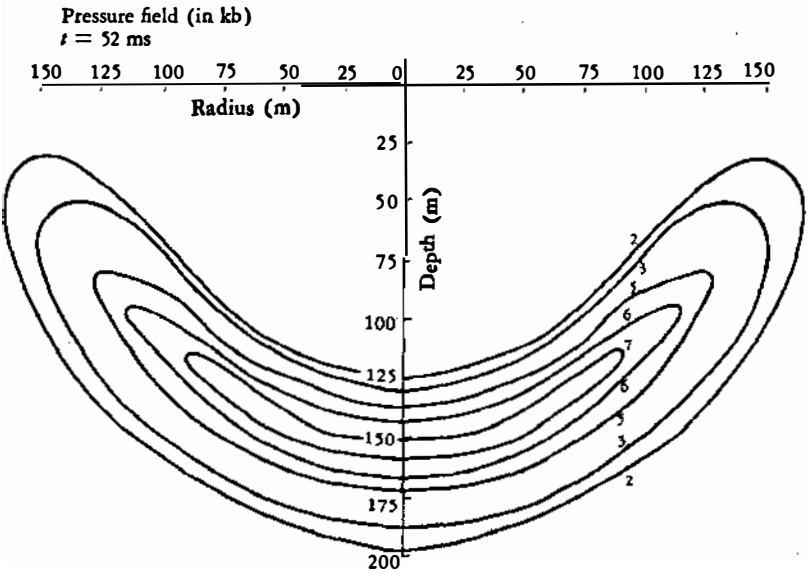

FIG. 35. Earth pressure contours from surface burst ($t = 52$ ms).

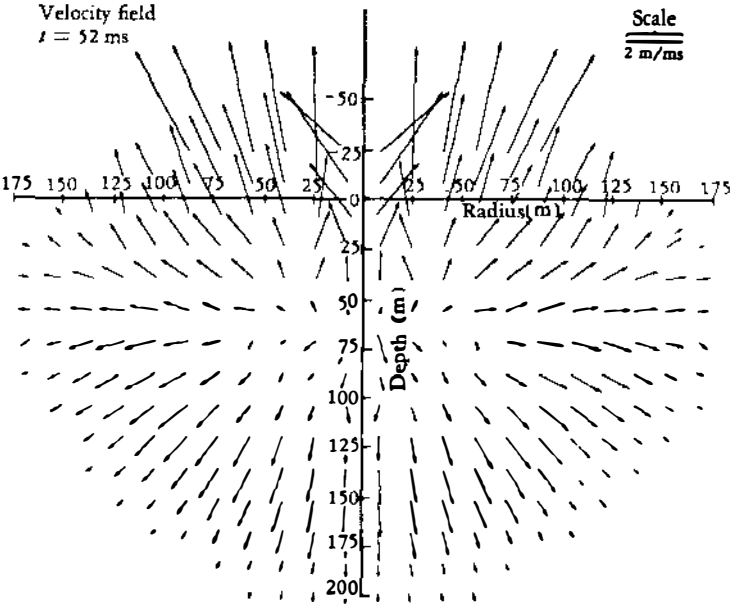

FIG. 36. Particle velocities from surface burst ($t = 52$ ms).

upward and downward motion at depths not unlike those representing the expected final crater profile.

DIRECT GROUND SHOCK

The extreme high stresses from a contained nuclear burst decrease rapidly with distance, this being somewhat dependent on the rock or soil into which it pushes. Figure 37 shows the peak stress versus range from a contained 1 MT in granite, tuff, and alluvium (dry). From the nature of the surface-burst calculated stress contours, it would appear profitable to compare the pressure versus range from contained bursts with the pressure versus depth below the surface bursts for a measure of relative efficiency. The surface burst begins with less effective energy, and continues to look less and less effective as the ground shock grows and exhausts more and more of its energy into the air above. Figure 38 presents some rather arbitrary bands of peak earth stress as functions of the depth below surface bursts of 1, 10, and 100 MT.

Note that the early decay of peak pressure follows an inverse cube of the slant distance from the burst point, as expected for a strong shock in any medium. At the lower pressures, the decay approaches a more gradual decay—more like the inverse square or inverse three-halves power of the radius. The pressures shown are intentional overestimates based largely on the hydrodynamic calculations. Experience with contained explosions indi-

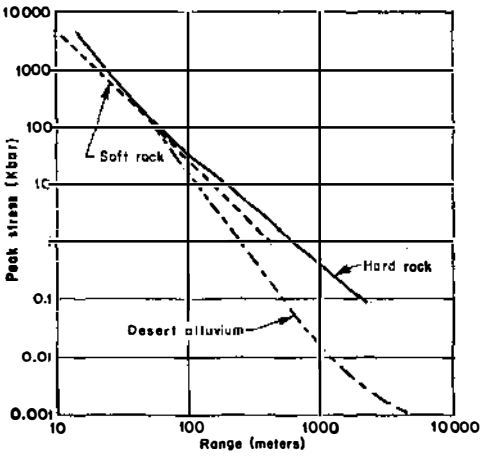

FIG. 37. Contained nuclear explosions peak stress versus range (1 MT).

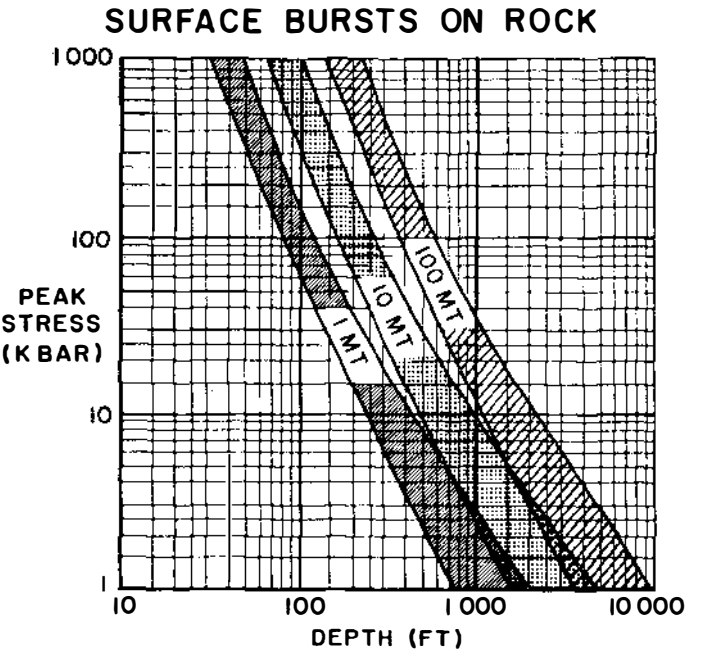

FIG. 38. Surface bursts on rock.

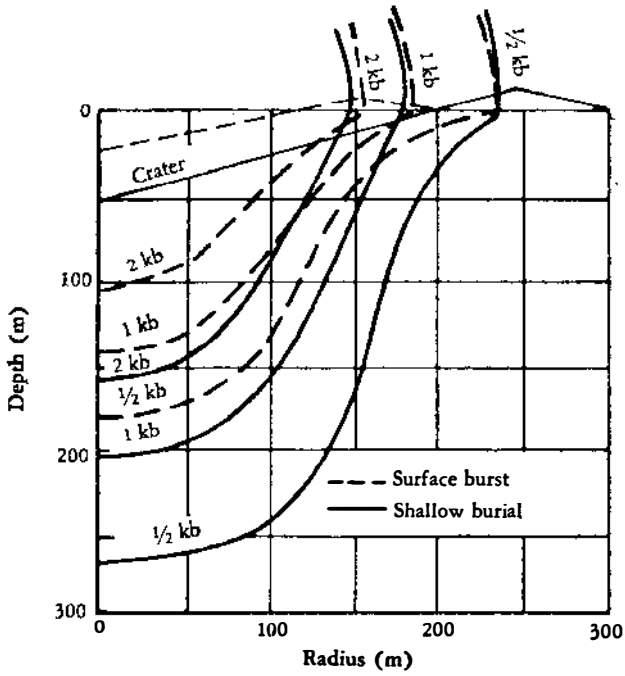

FIG. 39. Peak stress contours for 1 MT.

cates that other dissipative mechanisms provide an even more rapid decay of peak stress with distance.

Based in large part on these early calculations, Figure 39 shows peak stress contours for both a surface and a shallow-buried burst of 1 MT. The levels from ½ to 2 kb correspond to the onset of gross rock failures for most formations and thus represent the range of survival for the best examples of underground construction. From the relatively small lateral extent of these contours it is clear that a weapon must be delivered with great accuracy to be effective against a structure set deep in hard rock. Further, even a direct hit will not destroy an installation that is deep enough. Since these dimensions should increase no faster than as the cube root of the yield, an increase in attacking weapon yield does not rapidly require excessive depths of burial.

DEBRIS AND FALLOUT

The violently ejected crater material can be the source of much debris and some large, high-velocity ejecta as well as much of the dust and finer material that makes up the cloud and stem. In many burst conditions, the surface of the ground beyond the crater can provide a large volume of dust

and smoke to be carried aloft with the rising fireball. The reversed winds may be strong enough to bring back some debris to clog openings or revetments. These winds do not stop within a few seconds, but fade into the circulation set up by the rising fireball. The late fireball is still hot but at nearly normal pressure, so that its interior is at low density—forming a kind of buoyant balloon in the atmosphere. Figure 10 shows the densities versus radius at times as late as a few seconds. This several-thousand-foot-diameter, low-density sphere begins immediately to rise as a bubble as the denser air around it forces it upward. The rate of rise after a few seconds approaches 400 ft/sec. The circulation is such that the air velocities in the dust-laden stem that flows up through the rising cloud (Figure 14) are about twice the cloud-rise velocities, or as much as 800 ft/sec. The consequences of such wind velocities can be better appreciated when it is considered that the drag created by this flow could hold aloft a boulder weighing as much as 2 tons or could loft lesser rocks and debris to very high altitudes. An approximate empirical scaling for such winds and masses gives the following

$$\text{Upward velocity} \simeq 500 W^{1/4} \text{ ft/sec} \tag{54.}$$

$$\text{Supported spherical mass} \simeq 2^{-14} \eta^3 u^6 \text{ pounds} \tag{55.}$$

$$\simeq 300 \eta^3 W^{3/2} \text{ pounds} \tag{56.}$$

with W in MT, $\eta = \rho/\rho_0$.

The cloud continues to rise for 4 to 6 min, which can take it to altitudes over 60 000 ft, depending on meteorological conditions. Even after the cloud has stabilized, the stem continues to rise as the circulation persists. During the time of the initial cloud rise, much of cratered debris is aloft on various trajectories. Much of this material will be excavated at pressures below that needed to pulverize or vaporize the rock or soil, and some of it will be lofted in essentially its original sizes and shapes. If the soil is rocky, or if concrete and steel structures are involved, some large fragments must be expected at ranges at least as large as the stem radius; and there is some chance that rocks may rain down over a wide area for many minutes after a burst.

Again, if the wind circulation closely corresponds to the visible cloud and stem movements, wind velocities of the same order of magnitude ($\sim$100 ft/sec) may be expected at the base of the stem—i.e., in the dust-laden air above shelter.

Visibility will be restricted and unpredictable over an area corresponding to at least the 10-psi distance from such bursts, so that visual assessment of the postburst external environment will not always be possible. Direct human exposure would be undesirable, possibly even fatal, in the local fallout, which outside the immediate crater area (but within 10 miles or so) can rise to thousands of roentgens per hour in the first hour, falling to a few hundred at the end of a day. Total doses (integrated over time) after 18 hr may be in excess of 3000 roentgens over 1000 square miles. Clearly, surviving nearby surface installations or support structures will not be habitable for

many hours after a megaton-weapon surface burst, even in extreme emergencies. The extent and intensity of fallout depend critically on weapon design, details of burst position, and properties of soil and surrounding material. Although it is possible by design to enhance the radioactivity produced within a weapon, the height or depth of burst is more influential, and the nature of the cratered material is as important.

Slight burial can increase the intensity (while reducing the area coverage) of downwind fallout by severalfold over that from a surface burst, while even slight elevation above the surface can reduce manyfold the intensity (and area coverage) of local fallout. Most of these uncertainties are not reflected in fallout predictions, nor do such predictions consider the fact that higher-yield surface bursts are expected to excavate and carry aloft a mass or volume of earth less than proportional to the explosive yield. The radioactivity produced is roughly proportional to the fission fraction of the explosion yield, but the amount brought down in local or downwind fallout is determined by scavenging action of cratered material. Crater volumes increase less rapidly than linearly with increasing yields. The amount of debris available to bring to earth the vaporized atoms of the fission fragments is proportionately less for larger yields—particularly if the bursts are on or above the earth's surface.

In wartime situations with many bursts occurring, the fallout may be increased as the downwind plumes from various clouds cross and overlap.

LITERATURE CITED

1. Glasstone, S., Ed., *The Effects of Nuclear Weapons* (Rev. ed., U. S. Dept. Defense, USAEC, April 1962)
2. Brode, H. L., Asano, W., Stevenson, A., Plemmons, M., Scantlin, L., *A Program for Calculating Radiation Flow and Hydrodynamic Motion* (RAND Corp., RM-5187-PR, April 1967)
3. Gilmore, F. R., *Graphs of X-Ray Absorption Coefficients for Fourteen Substances* (RAND Corp., RM-2367-AEC, April 1959)
4. Hillendahl, R. W., *Theoretical Models for Nuclear Fireballs, DASA-1589, Part A* (Lockheed Missiles & Space Co., LMSC-B006750, August 1965)
5. Sachs, R. G., *The Dependence of Blast on Ambient Pressure & Temperature, Rept. 466* (Ballistic Res. Labs., May 1944)
6. Hilsenrath, J., Beckett, C. W., *Thermodynamic Properties of Argon-Free Air, Rept. 3991* (Natl. Bur. Std., April 1955)
7. Gilmore, R. R. (Private communication)
8. Freeman, B. E., *Opacity and Absorption Coefficients for Ionic Air, GAMD-4566* (Gen. Atomics, September 1963).
9. Gilmore, F. R., *A Table of the Planck Radiation Function and Its Integral* (RAND Corp., RM-1743, July 1956)
10. Glasstone, S., *op cit.*, 505
11. Sauer, F. M., *Nuclear Geoplosics*, **IV**, *DASA 1285* (Defense Atomic Support Agency, May 1964)
12. Perret, W. R., *Ground Motion Studies at High Incident Overpressure*, Operation Plumbbob, *WT-1405* (Sandia Corp., June 1960)
13. Brode, H. L., Bjork, R. L., *Cratering from a Megaton Surface Burst* (RAND Corp., RM-2600, June 1960)

CONTENTS